Received: 15 July 2019 | Accepted: 28 August 2019

DOI: 10.1111/gcb.14855

INVITED PRIMARY RESEARCH ARTICLE

Global Change Biology WILEY

# Simultaneous numerical representation of soil microsite production and consumption of carbon dioxide, methane, and nitrous oxide using probability distribution functions

Debjani Sihi[1] | Eric A. Davidson[1] | Kathleen E. Savage[2] | Dong Liang[3]

[1]Appalachian Laboratory, University of Maryland Center for Environmental Science, Frostburg, MD, USA

[2]Woods Hole Research Center, Falmouth, MA, USA

[3]Chesapeake Biological Laboratory, University of Maryland Center for Environmental Science, Solomons, MD, USA

**Correspondence and present address**
Debjani Sihi, Climate Change Science Institute, Environmental Sciences Division, Oak Ridge National Laboratory, 1 Bethel Valley Rd, Oak Ridge, TN 37830, USA.
Emails: sihid@ornl.gov; darisihi@gmail.com

**Funding information**
National Institute of Food and Agriculture, Grant/Award Number: 2014-67003-22073; USDA Forest Service's Northern Research Station; US Department of Energy's BER (Office of Science) Program

## Abstract

Production and consumption of nitrous oxide ($N_2O$), methane ($CH_4$), and carbon dioxide ($CO_2$) are affected by complex interactions of temperature, moisture, and substrate supply, which are further complicated by spatial heterogeneity of the soil matrix. This microsite heterogeneity is often invoked to explain non-normal distributions of greenhouse gas (GHG) fluxes, also known as hot spots and hot moments. To advance numerical simulation of these belowground processes, we expanded the Dual Arrhenius and Michaelis–Menten model, to apply it consistently for all three GHGs with respect to the biophysical processes of production, consumption, and diffusion within the soil, including the contrasting effects of oxygen ($O_2$) as substrate or inhibitor for each process. High-frequency chamber-based measurements of all three GHGs at the Howland Forest (ME, USA) were used to parameterize the model using a multiple constraint approach. The area under a soil chamber is partitioned according to a bivariate log-normal probability distribution function (PDF) of carbon and water content across a range of microsites, which leads to a PDF of heterotrophic respiration and $O_2$ consumption among microsites. Linking microsite consumption of $O_2$ with a diffusion model generates a broad range of microsite concentrations of $O_2$, which then determines the PDF of microsites that produce or consume $CH_4$ and $N_2O$, such that a range of microsites occurs with both positive and negative signs for net $CH_4$ and $N_2O$ flux. Results demonstrate that it is numerically feasible for microsites of $N_2O$ reduction and $CH_4$ oxidation to co-occur under a single chamber, thus explaining occasional measurement of simultaneous uptake of both gases. Simultaneous simulation of all three GHGs in a parsimonious modeling framework is challenging, but it increases confidence that agreement between simulations and measurements is based on skillful numerical representation of processes across a heterogeneous environment.

**KEYWORDS**

$CH_4$, $CO_2$, DAMM, DAMM-GHG, greenhouse gas, $N_2O$, probability distribution function, soil microsite

  

## 1 | INTRODUCTION

Fluxes of greenhouse gases (GHGs) from soil to the atmosphere are likely to play a significant role as biotic feedbacks to climate change (Ciais et al., 2014; Davidson & Janssens, 2006). Soils under forest, agriculture, and other land-use classes contribute to nearly a quarter of global emissions of GHGs, including carbon dioxide ($CO_2$), methane ($CH_4$), and nitrous oxide ($N_2O$; IPCC, 2014). Production and consumption of these biogenic GHGs are often associated with complex processes, involving carbon (C), nitrogen (N), and oxygen ($O_2$) substrates and inhibitors, and environmental controllers such as temperature, moisture, and transport of solutes and gases (Conrad, 1996), which remain challenging to simulate in ecosystem and earth system models (ESMs).

In this special issue, we present an expansion of a numerical soil process model that is a logical progression of several papers published by our group in the pages of this journal. While the importance of temperature on soil heterotrophic activity has been recognized for over a century (Arrhenius, 1889; Lloyd & Taylor, 1994; Vant't Hoff & Lehfeldt, 1899), and optima at intermediate values of soil moisture have also been well described (Hursh et al., 2017; Linn & Doran, 1984; Moyano, Manzoni, & Chenu, 2013), empirical relationships with these driving factors have had limited value in revealing a mechanistic understanding of soil respiration. Davidson, Belk, and Boone (1998) demonstrated that soil temperature and moisture had opposite seasonal trends in a moist temperate forest, resulting in confounding effects on soil respiration. Drawing on a growing body of research on soil respiration in the 1990s and 2000s, Davidson, Janssens, and Luo (2006) reviewed the emerging recognized need to move beyond mostly temperature functions, such as $Q_{10}$s, and to mechanistically link temperature and moisture drivers to substrate supply for soil heterotrophic respiration (Rh). Those concepts formed the basis of a parsimonious numerical model that used Dual Arrhenius and Michaelis–Menten (DAMM) kinetics to link soil temperature and moisture to their effects on substrate supply for soil respiration (Davidson, Samanta, Caramori, & Savage, 2012). In the 20 year special issue of this journal, Davidson, Savage, and Finzi (2014) described a vision for how the DAMM model could be conceptually linked to related processes of soil carbon dynamics, which has since been demonstrated in the modular Millennial Model (Abramoff et al., 2018), and how it could be integrated into large ecosystem models, which was since demonstrated by Sihi et al. (2018). Davidson et al. (2014) also proposed that other soil trace gas emissions could be simulated using the DAMM approach.

Here, we offer a new version of DAMM for the greenhouse gases, $CO_2$, $CH_4$, and $N_2O$ (hereafter, DAMM-GHG: Dual Arrhenius and Michaelis–Menten-Greenhouse Gas). We use three simultaneous data streams from chamber measurements of $CO_2$, $CH_4$, and $N_2O$ fluxes in a New England forest to constrain the DAMM-GHG model, which has a common structure for biophysical processes of production, consumption, and diffusion within the soil, including the contrasting effects of oxygen ($O_2$) as substrate or inhibitor for each process. Another innovation presented here is to represent soil microsite heterogeneity of soil carbon and moisture contents with probability distribution functions (PDFs) and to simulate the production and consumption of each gas at a microsite scale, rather than the traditional modeling approach of using bulk soil means of measured carbon and moisture as model drivers.

Thermodynamic theories suggest that $CH_4$ oxidation (aka methanotrophy) should proceed under aerobic conditions and $CH_4$ production (aka methanogenesis) should be favored under anaerobic (or reducing) conditions (Conrad, 2009; Dean et al., 2018). Production of $N_2O$ via nitrification and denitrification processes is known to peak at an optimal intermediate soil moisture content, whereas reducing soil conditions under high water content are thought to be prerequisites for $N_2O$ reduction to $N_2$ via classical denitrification (Butterbach-Bahl, Baggs, Dannenmann, Kiese, & Zechmeister-Boltenstern, 2013; Davidson, 1991; Firestone & Davidson, 1989). While a large body of literature generally supports these patterns, there are exceptions that are frequently attributed to spatial heterogeneity within soils and soil microsites.

While the highest rates of net consumption of atmospheric $N_2O$ (i.e., $N_2O$ reduction) is observed in wetlands, $N_2O$ reduction in well-drained upland soils has been observed sporadically for many years (Chapuis-Lardy, Wrage, Metay, Chotte, & Bernoux, 2007; Schlesinger, 2013; Syakila, Kroeze, & Slomp, 2010). Such observations have often been discounted as measurement error or noise. The recent advent of fast response field instruments with good sensitivity and precision has permitted confirmation that upland soils can be small sinks of $N_2O$ (Eugster et al., 2007; Savage, Phillips, & Davidson, 2014), and a modest soil sink for atmospheric $N_2O$ is now generally accepted as plausible for some sites and times. Increasing soil sink strength of $N_2O$ during drought events further increases perplexity, given that drought events generally facilitate soil aeration (Goldberg & Gebauer, 2009). Occasional observations of net emissions of $CH_4$ from well-drained upland soils, although contrary to expectations, are also common (Brewer, Calderón, Vigil, & Fischer, 2018; Cattânio, Davidson, Nepstad, Verchot, & Ackerman, 2002; Keller & Matson, 1994; Silver, Lugo, & Keller, 1999; Teh, Silver, & Conrad, 2005; Verchot, Davidson, Cattânio, & Ackerman, 2000).

Spatial heterogeneity of soil microsites is often invoked to explain net atmospheric uptake of $N_2O$ and net emissions of $CH_4$ from well-drained upland soils. Soil heterogeneity at microscales can cause a wide range of microsite redox potentials and concentrations of substrates, which must be accounted for to explain highly skewed distributions of soil GHG fluxes (Parkin, 1987, 1993; Savage et al., 2014; Stoyan, De-Polli, Böhm, Robertson, & Paul, 2000). Because existing ESMs are not able to represent the underlying mechanisms that control variation in enzymatic processes at microsite scales (Tian et al., 2019; Xu et al., 2016), these models often fail to capture the dynamics of soil GHG fluxes, including the so-called hot spots and hot moments (Groffman, 2012; Groffman et al., 2009; Lurndahl, 2016; Saha et al., 2018) or control points (Bernhardt et al., 2017).

Only recently have modeling activities at ecosystem (or landscape) scales begun to shift from the classical framework based on redox strata (or water table position) and mean measured soil

moisture to emerging conceptual frameworks that consider heterogeneous environment for production and consumption of GHGs (Ebrahimi & Or, 2018; Keiluweit, Gee, Denney, & Fendorf, 2018; Or, 2019; Wang, Brewer, Shugart, Lerdau, & Allison, 2019; Yang et al., 2017). However, to our knowledge, mechanistic simulation of simultaneous production, consumption, and diffusion of multiple gases ($CO_2$, $CH_4$, $N_2O$, and $O_2$) among multiple soil microsites has not yet been attempted. Numerical representation of microsite production and consumption of multiple GHGs is necessary to simulate concurrent $N_2O$ reduction and $CH_4$ oxidation processes in well-drained upland soils (Savage et al., 2014). The overall objective of this work is to demonstrate that the qualitative explanations of microsite heterogeneity can be expressed in a mathematically consistent biophysical process model that is numerically consistent with simultaneously measured fluxes of all three GHGs: $CO_2$, $CH_4$, and $N_2O$.

While originally developed for aerobic Rh, here we expand the original core structure of the DAMM model (Davidson et al., 2012, 2014; Figure S1) to represent methanogenesis, methanotrophy, $N_2O$ production, and $N_2O$ reduction reactions using the same framework and physics for simulating the availability of $O_2$ and other substrates and for diffusion of gases across soil–atmosphere boundary using microsite PDFs (Figure 1; Figure S1). Simultaneously constraining our GHG enzyme kinetic model (i.e., DAMM-GHG) with observations of fluxes of multiple GHGs presents large challenges, because tuning a model to agree with one data stream may cause a poorer fit to a second or third data stream. However, if all data streams can be simultaneously simulated with adequate fidelity and skill, this multiple

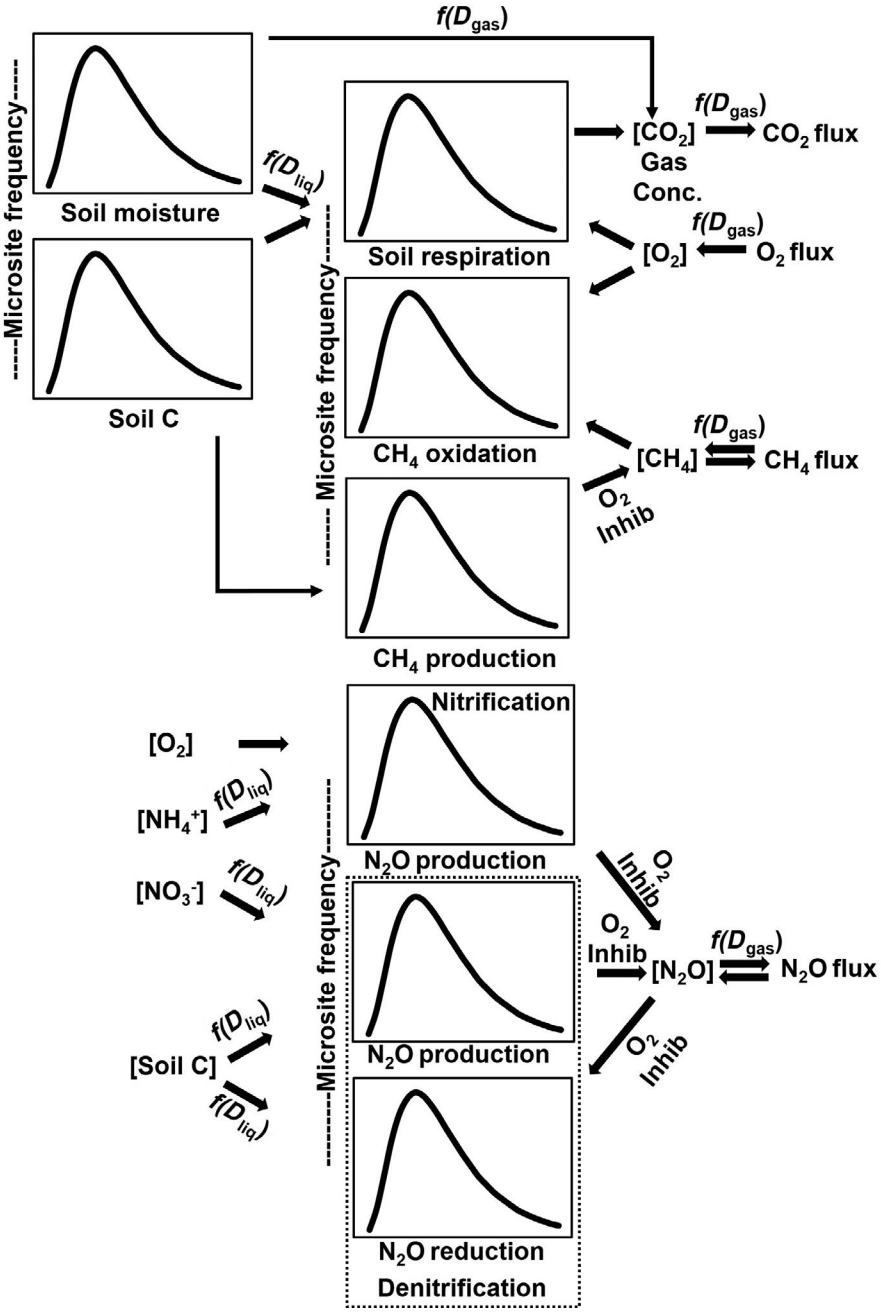


**FIGURE 1** Conceptual framework for simultaneous representation of $CO_2$, $CH_4$, and $N_2O$ fluxes in DAMM-GHG model. Inhib represents inhibition. $f(D_{gas})$ and $f(D_{liq})$ represent soil moisture effect on diffusion of gases and soluble substrates, respectively

constraint approach enhances the probability that the parameterization and process representations are realistic and robust. One can never be certain that a model gets the "right answer for the right reason," but challenging a single model with multiple data streams of related but differing processes, such as $CO_2$, $CH_4$, and $N_2O$ fluxes, confers additional credence to its structure and parameterization.

## 2 | MATERIALS AND METHODS

### 2.1 | Site description and data collection

We measured GHG fluxes in a mature boreal-transition forest with a hummock–hollow microtopography, Howland Forest research site (45.20°N, 68.74°W) from central Maine, United States. Mean annual temperature and mean annual precipitation are +5.5°C and 1,000 mm, respectively. Soils of the Howland Forest upland sites are characterized as Skerry fine sandy loam, frigid Aquic Haplorthods. More information on the Howland Forest research site can be found in Fernandez, Rustad, and Lawrence (1993).

High-frequency (sampling frequency: 1 Hz) real-time soil $CH_4$ and $N_2O$ fluxes were measured using an Aerodyne quantum cascade laser integrated with soil $CO_2$ flux measurements by LI-COR IRGA assembly. Triplicate chambers were each sampled once every 2 hr. Chamber tops were closed for 5 min and automated fluxes were calculated by fitting a linear regression on the change in headspace GHG concentrations followed by temperature and pressure corrections. We characterized the uncertainty of measurements by the standard deviation estimates for all three GHGs. Soil temperature and soil moisture were measured at each chamber location at 10 cm depth once every hour using a Type-T thermocouple and Campbell Scientific CS616 water content reflectometer probes, respectively, and stored on a Campbell Scientific CR10X data logger (Campbell Scientific). We used daily average values of both drivers (soil temperature and soil moisture) and GHG fluxes for modeling purposes to smooth high measurement noise observed at subdaily timescale. See Savage and Davidson (2003) for more details on our chamber design and automated sampling system. Quality control protocols for soil GHG fluxes can be found in Savage, Davidson, and Richardson (2008) and Savage et al. (2014).

### 2.2 | Modeling scheme

Aerobic and anaerobic processes in soil are linked through heterotrophic dependence on fixed C sources for energy, but with contrasting effects of $O_2$ as either essential substrate or potential inhibitor (Figure 1; Figure S1). To date, most biogeochemical models use separate model versions for simulating soil organic matter decomposition resulting in $CO_2$ emissions and the processes affecting $CH_4$ and $N_2O$ emissions, but here we simultaneously simulate biogeochemically linked multiple GHG emissions using the same biophysical framework.

For the present study, we focus primarily on Rh being the dominant source of $CO_2$ production and fate of $O_2$ consumption, with the resulting $O_2$ concentrations then affecting the net fluxes of $CH_4$ and $N_2O$ by methanogenesis, methanotrophy, nitrification, and denitrification processes. The logic for coupled simulation of $CO_2$, $CH_4$, and $N_2O$ fluxes in the DAMM-GHG model, illustrated in Figure 1, is as follows:

1. The measured soil C and soil moisture can be partitioned according to a simulated log-normal PDF, such as a distribution where only a small fraction of microsites has high soil C or high soil moisture.
2. Log-normal PDFs of soil C substrates and soil moisture among microsites lead to a simulated PDF of Rh, applying the original DAMM model independently to each microsite within the PDF.
3. Simulated microsite $CO_2$ production is aggregated to the chamber scale to estimate Rh contributing to the chamber flux measurement. We then estimate the total soil $CO_2$ flux by adding the contribution of root-derived $CO_2$ fluxes to Rh based on previously measured ratios at the Howland Forest (Carbone et al., 2016; Savage, Davidson, Abramoff, Finzi, & Giasson, 2018; Sihi et al., 2018). A distinct seasonal pattern of the contribution of root-derived $CO_2$ (Ra) to total soil $CO_2$ fluxes (SR) increased from 0.50 in early spring to around 0.65 in early autumn, followed by a declining trend through winter (Figure S2). Total chamber-based measurements of $CO_2$ efflux are used as a constraint for the sum of the simulated root and heterotrophic $CO_2$ production rates across the simulated PDF of microsites.
4. The simulated and measured soil $CO_2$ efflux is a reasonable proxy for $O_2$ demand within the soil. The respiration quotient is not exactly unity, but is usually close enough to unity in noncalcareous soils to allow simulation of $O_2$ consumption within the soil based on measurement-constrained simulated $CO_2$ efflux (Angert et al., 2015). Knowledge of respiration quotient would be needed for the application of our DAMM-GHG model to calcareous soils. We assumed that the simulation of $O_2$ consumption by the original version of the DAMM model serves our purpose of estimating the $O_2$ demand (or consumption) here (see Figure S1).
5. Microsite PDFs of $O_2$ concentrations are then simulated as a function of $O_2$ consumption rates distributed across microsites and gaseous diffusion rates using the same DAMM functions in Figure S1 driven by air-filled porosity.
6. Next, the resulting PDF of $O_2$ concentrations is used to simulate methanogenesis, methanotrophy, $N_2O$ production, and $N_2O$ consumption at the scale of each of the distributed microsites according to similar Michaelis–Menten and diffusion equations (Figure S1), where $O_2$ serves as either inhibitor or substrate (Davidson et al., 2014). The net $CH_4$ and $N_2O$ flux summed across simulated PDFs of microsites are constrained by observed chamber-based fluxes of $CH_4$ and $N_2O$.

We used soluble C as a proxy for the reducing power needed for methanogenesis. However, future studies may explicitly represent specific substrates for acetoclastic and hydrogenotrophic methanogenic pathways, if parameterization of that type of model structure can be constrained by the availability of data on concentrations of organic acids

(acetate, formate) and hydrogen ($H_2$), which was not the case for our study. We also assumed that respiration is the dominant pathway of $CO_2$ production in soil. Thus, we did not account for the minor contribution of acetoclastic methanogens to $CO_2$ production and hydrogenotrophic methanogens to $CO_2$ consumption. Likewise, we considered soil respiration is the major sink of $O_2$ and ignored the otherwise small fraction of $O_2$ consumed by methanotrophs.

We added a nitrification module to account for the $N_2O$ production during nitrification using the observed seasonal dynamics of ammonium ($NH_4^+$) in our study area (Fernandez, Lawrence, & Son, 1995). The Howland Forest is a strongly nitrogen-limited system, with porewater nitrate ($NO_3^-$) concentration always close to detection limits by inductively coupled plasma-mass spectrometry, ICP-MS (Fernandez et al., 1995). $N_2O$ production during classical denitrification is mechanistically simulated using seasonally averaged porewater $NO_3^-$ data along with microsite PDFs of soil C and soil moisture. Nitrous oxide is reduced to $N_2$ during classical denitrification following the Hole-in-the-Pipe conceptual model, including possible reduction of atmospheric $N_2O$ that diffuses into the soil (Firestone & Davidson, 1989). See Supporting Information (Section S2) for DAMM-GHG model equations.

## 2.3 | Microsite probability distribution functions of soil C and soil moisture

The microsite PDFs of soil C substrate and soil moisture were generated from a bivariate truncated log-normal distribution. The PDF for soil C was truncated at 0.001 and 0.15 ($g/cm^3$), respectively. The soil C PDF was distributed with mean equaling the observed soil C value (see Figure S3 for more information on the PDF of soil C). Likewise, the soil moisture PDF was distributed with mean equaling the observed soil moisture value, truncations at 70% and 200% of the observed mean soil moisture values. The spatial heterogeneity of soil C and soil moisture were constrained by optimizing the parameters (standard deviation and/or coefficient of variation) that control the skewness of soil C and soil moisture PDFs by enveloping the bounds reported by Stoyan et al. (2000). If the upper truncation limit of the soil moisture PDF exceeded the soil pore volume, we reset it to 95% of the porosity value. We constructed the microsite PDF as the product of two log-normal distributions of soil C and soil moisture. The PDF was evaluated at 10 × 10 equally spaced quantiles for soil C and soil moisture, respectively.

Here, we focused on spatial heterogeneity across soil microsites at the mm and sub-mm scale. Within stand heterogeneity at the meter scale, such as variation in bulk density and porosity along topographical gradients, is not account for in this study.

## 2.4 | Parameter optimization and uncertainty analysis

We optimized model parameters within a Bayesian Markov chain Monte Carlo (MCMC) framework (see Section S1 for more details on the optimization algorithm). We implemented the MCMC algorithm using *mcmc* and *doParallel* packages (Revolution Analytics & Weston, 2015) in the R (version 3.3.2) statistical programming language (R Core Team, 2018). We applied a posterior predictive procedure to estimate the uncertainty of the optimized parameters. We implemented the posterior predictive analyses using the *R-INLA* package (Lindgren & Rue, 2015; Rue, Martino, & Chopin, 2009). We divided daily-average soil GHG flux measurements into alternative synoptic-scale periods of 10 days, where we used one half of measured GHG fluxes for model calibration and another half for model validation.

## 2.5 | Sensitivity analysis

We evaluated the sensitivity of model parameters using a global variance-based sensitivity analysis and a collinearity (or parameter identifiability) analysis. We implemented a variance-based sensitivity analysis using the R-*multisensi* package, where a generalized sensitivity index (ranging between 0 and 1, extracted from the first axis of principle component analysis) was used to determine the sensitivity of multiple GHG fluxes to each model parameter value (Bidot, Lamboni, & Monod, 2018). The global sensitivity analysis quantifies the proportion of variability accounted by each of the parameters on model outputs, where a high GSI value indicates that the simulation results are highly sensitive to that parameter (Lamboni, Makowski, Lehuger, Gabrielle, & Monod, 2009).

We implemented the collinearity analysis using the *collin* function of *R-FME* package, where the collinearity index (CI) was used to determine the linear dependence of model parameters to each other (Brun, Reichert, & Künsch, 2001; Soetaert, 2016; Soetaert & Petzoldt, 2010). In general, higher values of CI indicate increased equifinality (or decreased number of identifiable parameters) of model parameters. One can compensate $\left(1-{}^{1}/_{\mathrm{CI}}\right)$ % of the effect of a change in one parameter by modifying the values of other parameters. Hence, CI values can range between 1 (when all terms are orthogonal or all subsets of parameters are identifiable) and infinity (when all terms are linearly dependent, or no single subset of parameters is identifiable). The CI value of 15 is considered as a threshold above which approximate linear dependence of model parameters increases and poor identifiability can be expected (sensu Omlin, Brun, & Reichert, 2001).

# 3 | RESULTS

## 3.1 | Seasonality of soil greenhouse gas fluxes

Soil $CO_2$ fluxes followed the typical seasonal trend of soil temperature, where both seasonal average and peak $CO_2$ fluxes were comparable between 2015 (average [min–max]: 171 [73–297] mg $CO_2$-C $m^{-2}$ $hr^{-1}$) and 2016 (average [min–max] measurement period: 168 [52–281] mg $CO_2$-C $m^{-2}$ $hr^{-1}$; Figure 2). This is due, in part, to the comparable seasonal soil temperature ranges between 2015

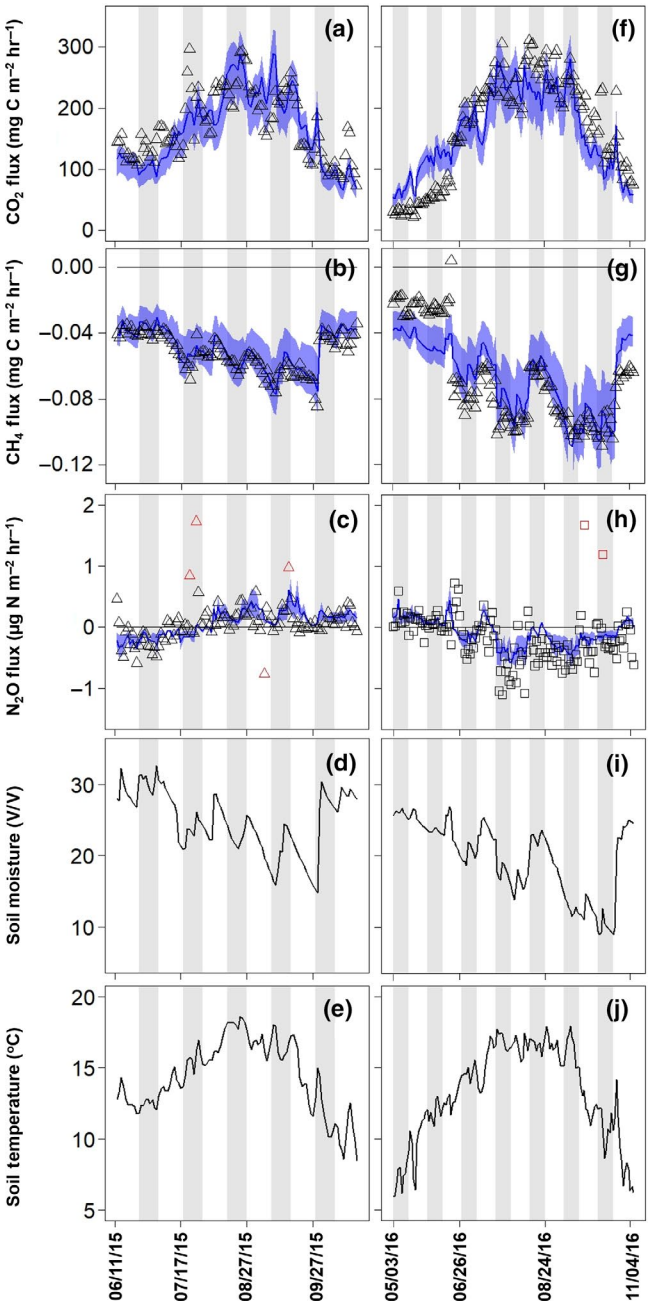


**FIGURE 2** Temporal trend of greenhouse gas, GHG ($CO_2$: a, f; $CH_4$: b, g; and $N_2O$: c, h) fluxes, soil moisture (d, i), and soil temperature (e, j) during 2015 (a–e) and 2016 (f–j) growing seasons. Triangles and squares represent observed GHG fluxes in 2015 and 2016, respectively. Light gray shades in the background represent validation windows, which are interspersed throughout the observation period. Red triangles and squares represent outliers for $N_2O$ fluxes. Blue line and shade represent median and 95% CI of simulated GHG fluxes, respectively

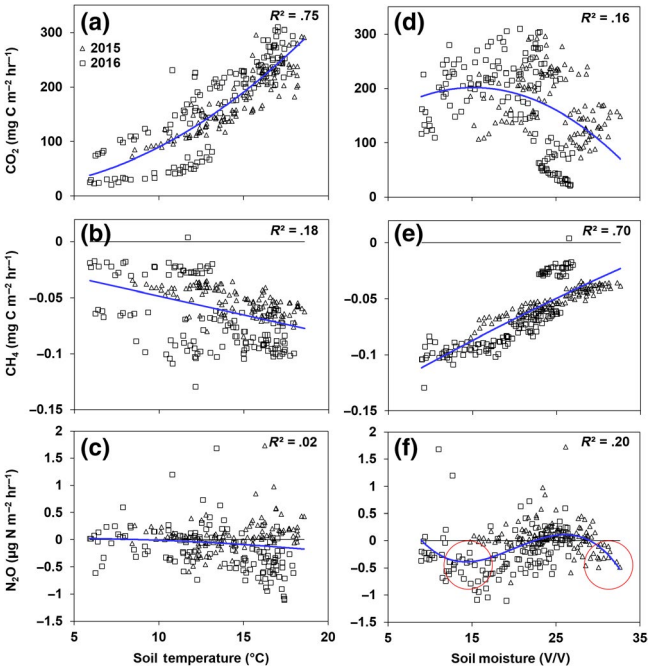


**FIGURE 3** Relation of observed $CO_2$ (a, d), $CH_4$ (b, e), and $N_2O$ (c, f) fluxes with soil temperature (a–c) and soil moisture (b–e). Triangles and squares represent observed GHG fluxes in 2015 and 2016, respectively

(average: 14.4°C, ranged between 8.4 and 18.6°C) and 2016 (average: 13.3°C, ranged between 5.6 and 17.9°C) measurement periods (Figures 2 and 3). Soil $CO_2$ fluxes exponentially increased with soil temperature ($R^2$ = .75; Figure 3a). We also observed a typical bell-shaped relationship between $CO_2$ flux and soil moisture ($R^2$ = .16), with the optimum for $CO_2$ flux at intermediate water contents (Figure 3d). Although the effect of soil moisture on $CO_2$ fluxes was always secondary to soil temperature (Figure S5), the fit with soil moisture was better when it was more limiting in the dry summer of 2016 than the wet summer of 2015 ($R^2$ = .24 and .52 in 2015 and 2016, respectively; Figure S6d).

In contrast to $CO_2$ fluxes, soil $CH_4$ fluxes mimicked the seasonal trend of soil moisture for both years (Figure 2b,g). Soil moisture and net $CH_4$ fluxes were positively related ($R^2$ = .70), although the slope of the linear regression line was steeper during 2016 than during 2015 (Figure 3e; Figure S6e). We observed relatively smaller net $CH_4$ oxidation in the spring followed by higher net $CH_4$ oxidation in summer months, and again lower net $CH_4$ oxidation in the autumn. Although seasonal average values were generally similar, the range of $CH_4$ flux values in 2016 (average: −0.07 μg $CH_4$-C $m^{-2}$ $hr^{-1}$, min–max range: −0.13 to 0.004 μg $CH_4$-C $m^{-2}$ $hr^{-1}$) was wider than in 2015 (average: −0.05 μg $CH_4$-C $m^{-2}$ $hr^{-1}$, min–max range: −0.08 to −0.03 μg $CH_4$-C $m^{-2}$ $hr^{-1}$).

Unlike $CO_2$ and $CH_4$, the seasonal trend of soil $N_2O$ fluxes contrasted between 2015 and 2016 (Figures 2c,h and 3f; Figure S6f). The 2015 growing season was significantly wetter than the 2016 growing season. The cumulative precipitation of the summer months (June 1 to September 30) of 2015 and 2016 was 439 mm and 279 mm, respectively (source: https://www.ncdc.noaa.gov/crn/). Consequently, the average soil moisture was generally higher (24.8 v/v, min–max range: 14.8–32.6 v/v) during the 2015 growing season (measured over June 11 to October 17) than the average soil moisture (19.7 v/v, min–max range: 8.9–27 v/v) during the 2016 growing season (measured over May 3 to November 6; Figures 2d,i and 3f; Figure S6f).

We observed low rates of net $N_2O$ consumption during the spring of 2015 when soil moisture was highest, which was followed by mostly near zero net emissions and a few positive emissions throughout the 2015 summer (Figure 2c,d). In contrast, we observed net positive $N_2O$ emission during the early spring of 2016 and net $N_2O$ consumption throughout most of the 2016 growing season, when soil moisture was minimal (Figure 2h,i). The temperature effect was weak and inconsistent between 2 years (Figure 3c; Figure S6c). On average, we observed small net $N_2O$ emission during the 2015 growing season (average: 0.06 μg $N_2O$-N $m^{-2}$ $hr^{-1}$, ranged between −0.77 and 1.73 μg $N_2O$-N $m^{-2}$ $hr^{-1}$) and net $N_2O$ consumption during the 2016 growing season (average: −0.18 μg $N_2O$-N $m^{-2}$ $hr^{-1}$, ranged between −1.10 and 1.68 μg $N_2O$-N $m^{-2}$ $hr^{-1}$).

## 3.2 | Performance of the DAMM-GHG model

Overall, the model reproduced the seasonal dynamics of soil greenhouse gas fluxes (Figures 2 and 4). The model explained 72% of the variation in soil $CO_2$ fluxes (Figure 4a). Likewise, the 1:1 relation

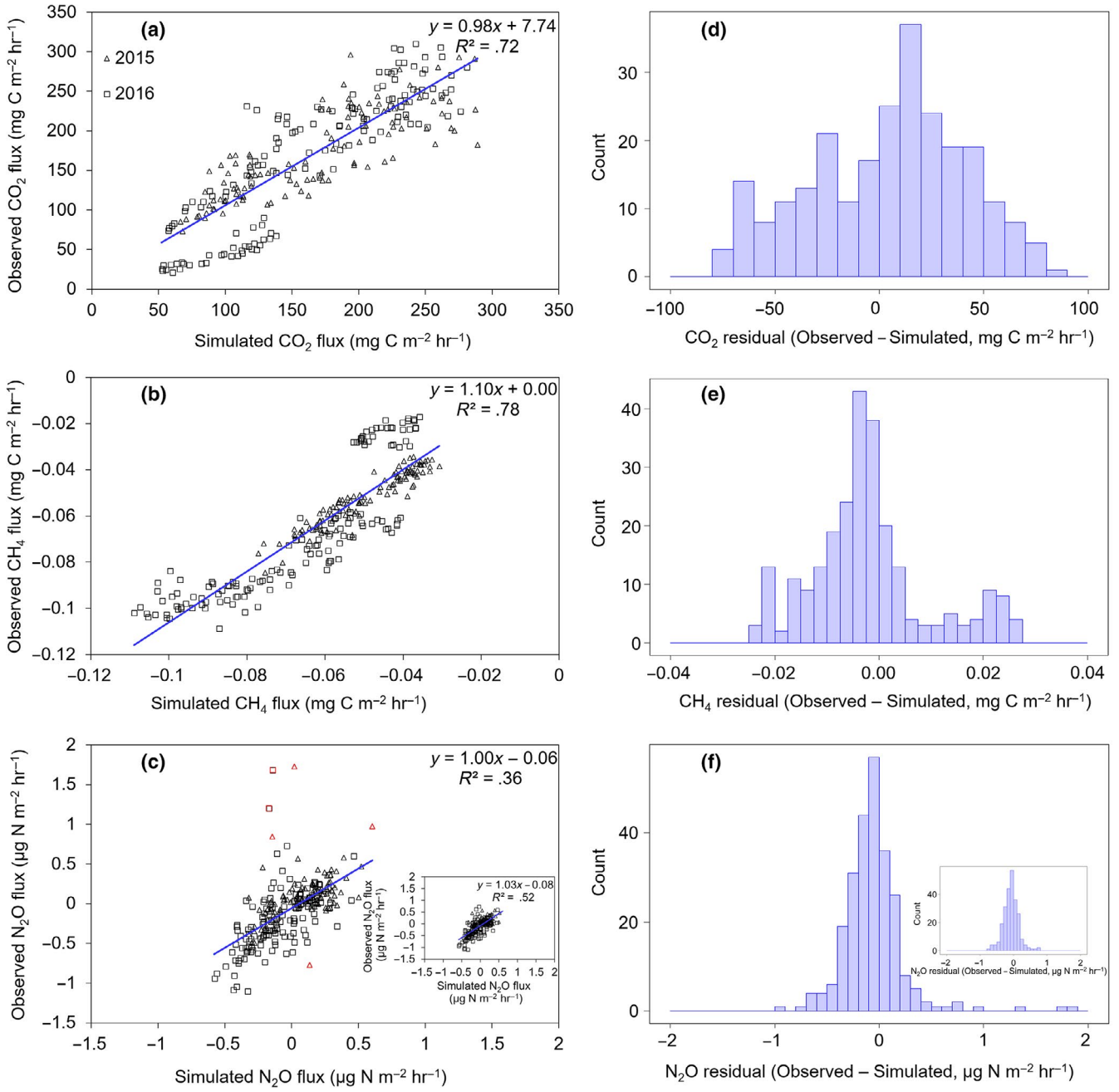


**FIGURE 4** Relation between observed versus simulated greenhouse gas, GHG ($CO_2$: a, d; $CH_4$: b, e; and $N_2O$: c, f) fluxes. Triangles and squares in (a–c) represent observed GHG fluxes in 2015 and 2016, respectively. Red triangles and squares in lower left panel (c) represent outliers for $N_2O$ fluxes. Inset figures in bottom panels (c, f) represent one-to-one relation and model residuals for $N_2O$ after removing the outliers

**TABLE 1** Parameters used for simultaneous simulation all three greenhouse gases in the DAMM-GHG model

| Parameter | Description | Unit | Prior range | Posterior range | Source |
|---|---|---|---|---|---|
| *For $CO_2$ module* | | | | | |
| $\alpha_{CO_2}$ | Base rate for soil respiration | μmol $CO_2$ $L^{-1}$ $hr^{-1}$ | $2 \times 10^{10}$ ($2 \times 10^{9}$–$2 \times 10^{11}$) | $5 \times 10^{9}$ ($2 \times 10^{9}$–$9 \times 10^{9}$) | Abramoff et al. (2017), Davidson et al. (2018), Sihi et al. (2018) |
| $E_{a_{CO_2}}$ | Temperature sensitivity for soil respiration | kJ/mol | 72 (60–80) | 66 (64–72) | |
| $kM_{C\text{-}CO_2}$ | Half-saturation constant of C for soil respiration | μmol C/L | 1 (0.1–100) | 0.9 (0.7–1.6) | |
| $kM_{O_2\text{-}CO_2}$ | Half-saturation constant of $O_2$ for soil respiration | μmol $O_2$/L | 100 (3–300) | 16 (4–38) | |
| Depth | Effective depth | cm | 15 (5–30) | 7 (6–11) | This study |
| Total microsite | Total number of microsites | unitless | $10^4$ ($10^3$–$10^5$) | $7 \times 10^3$ ($2 \times 10^3$–$9 \times 10^3$) | This study |
| Soil $C_{SD}$ | Coefficient that determines skewness of soil carbon PDF | unitless | 0.5 (0.1–0.9) | 0.5 (0.1–0.9) | Stoyan et al. (2000) |
| Soil $moisture_{SD}$ | Coefficient that determines skewness of soil moisture PDF | % | 20 (5–30) | 7 (6–12) | Stoyan et al. (2000) |
| *For $CH_4$ module* | | | | | |
| $\alpha_{CH_4prod}$ | Base rate for $CH_4$ production | μmol $CH_4$ $L^{-1}$ $hr^{-1}$ | $3 \times 10^5$ ($3 \times 10^4$–$3 \times 10^6$) | $3 \times 10^5$ ($2 \times 10^5$–$6 \times 10^5$) | This study |
| $E_{a_{CH_4prod}}$ | Temperature sensitivity for $CH_4$ production | kJ/mol | 100 (50–150) | 74 (68–78) | Nedwell and Watson (1995), Westermann (1993) |
| $kM_{C\text{-}CH_4}$ | Half-saturation constant of C for $CH_4$ production | μmol C/L | 1 (0.1–100) | 1.2 (0.9–2.1) | This study |
| $kI_{CH_4}$ | Inhibition coefficient of $O_2$ for $CH_4$ production | μmol $O_2$/L | 3 (0.3–4.3) | 0.43 (0.4–0.9) | Arah and Stephen (1998) |
| $\alpha_{CH_4ox}$ | Base rate for $CH_4$ oxidation | μmol $CH_4$ $L^{-1}$ $hr^{-1}$ | 0.07 (0.007–7) | 0.1 (0.08–2) | Davidson et al. (2001) |
| $E_{a_{CH_4ox}}$ | Temperature sensitivity for $CH_4$ oxidation | kJ/mol | 30 (10–50) | 34 (32–37) | Crill, Martikainen, Nykanen, and Silvola (1994) |
| $kM_{CH_4}$ | Half-saturation constant of $CH_4$ for $CH_4$ oxidation | μmol $CH_4$/L | $10^{-2}$ ($10^{-3}$ to $10^{-1}$) | 0.005 (0.002–0.006) | Davidson et al. (2001) |
| $kM_{O_2-CH_4}$ | Half-saturation constant of $O_2$ for $CH_4$ oxidation | μmol $O_2$/L | 43 (3–300) | 24 (13–33) | Davidson et al. (2001) |
| *For $N_2O$ module* | | | | | |
| $\alpha_{N_2O_{prod\text{-}nitrif}}$ | Base rate for nitrification | μmol $N_2O$/L | $10^2$ ($10^1$–$10^3$) | 282 (207–722) | This study |
| $E_{a_{N_2O_{prod\text{-}nitrif}}}$ | Temperature sensitivity for $N_2O$ production during nitrification | kJ/mol | 60 (45–75) | 62 (57–67) | Stark (1996), Stark and Firestone (1996) |
| $kM_{NH_4}$ | Half-saturation constant of $NH_4^+$ for $N_2O$ production | μmol $NH_4^+$/L | 15 (8–22) | 9 (8–10) | Stark and Firestone (1996), Zarnetske, Matsuo, Yamazaki, and Wada (1987) |

(Continues)

**TABLE 1** (Continued)

| Parameter | Description | Unit | Prior range | Posterior range | Source |
|---|---|---|---|---|---|
| $kM_{O_2\text{-}N_2O}$ | Half-saturation constant of $O_2$ for $N_2O$ production | μmol $O_2$/L | 100 (9–163) | 36 (15–44) | Bodelier, Libochant, Blom, and Laanbroek (1996), Verstraete and Focht (1977), Zarnetske et al. (1987) |
| $\alpha_{N_2O_{prod\text{-}denitrif}}$ | Base rate for $N_2O$ production | μmol $N_2O$/L | $10^2$ ($10^1$–$10^3$) | 520 (438–958) | This study |
| $E_{a_{N_2O_{prod\text{-}denitrif}}}$ | Temperature sensitivity for $N_2O$ production during denitrification | kJ/mol | 60 (45–75) | 67 (65–71) | Canion et al. (2014), Holtan-Hartwig, Dörsch, and Bakken (2002), Vieten (2008) |
| $kM_{NO_3}$ | Half-saturation constant of $NO_3^-$ for $N_2O$ production | μmol $NO_3^-$/L | 26 (15–57) | 17 (16–19) | Zarnetske et al. (1987) |
| $kI_{N_2O-prod}$ | Inhibition coefficient of $O_2$ for $N_2O$ production | μmol $O_2$/L | 14.3 (4.3–43) | 41 (40–42) | Körner and Zumft (1989), Zarnetske et al. (1987) |
| $kM_{C\text{-}N_2O}$ | Half-saturation constant of C for $N_2O$ production and reduction during denitrification | μmol C/L | 1 (0.1–100) | 0.6 (0.3–1) | This study |
| $\alpha_{N_2O_{red}}$ | Maximum velocity for $N_2O$ reduction | μmol $N_2O$/L | $10^3$ ($10^2$–$10^4$) | 3,413 (1,585–9,583) | This study |
| $E_{a_{N_2O_{red}}}$ | Temperature sensitivity for $N_2O$ reduction | kJ/mol | 50 (45–75) | 47 (46–47) | Canion et al. (2014), Holtan-Hartwig et al. (2002), Vieten (2008) |
| $kM_{N_2O}$ | Half-saturation constant of $N_2O$ for $N_2O$ reduction | μmol $N_2O$/L | 0.16 (0.05–0.27) | 0.19 (0.13–0.26) | Holtan-Hartwig et al. (2002), Vieten (2008) |
| $kI_{N_2O\text{-}red}$ | Inhibition coefficient of $O_2$ for $N_2O$ reduction | μmol $O_2$/L | 7.5 (4.3–20.1) | 19.5 (18.6–19.7) | Körner and Zumft (1989), Vieten (2008) |

*Note:* Prior range represents initial (min–max) of prior interquartile range. Posterior range represents median (95% CI) of posterior interquartile range. Units for all base rates, that is, $\alpha$(s), are in μmol concentration dissolved in water.

Abbreviation: PDF, probability distribution function.

between the observed and simulated soil $CH_4$ fluxes was remarkable ($R^2$ = .78; Figure 4b). The model marginally overestimated $CO_2$ fluxes and underestimated $CH_4$ fluxes during early spring of 2016 (Figure 2f,g).

Soil $N_2O$ fluxes were relatively noisier as compared to $CO_2$ and $CH_4$ fluxes with a few outliers in both years (red triangles and squares in Figures 2 and 4, respectively). The model generally explained the dynamics of $N_2O$ fluxes ($R^2$ = .36 and .52 with and without outliers, respectively; Figure 4c). The model did not capture the few very low net $N_2O$ fluxes observed in the peak season of 2016. Most importantly, the model captured the instances when net atmospheric consumption of $CH_4$ (i.e., net $CH_4$ oxidation) co-occurred with net atmospheric consumption of $N_2O$ (i.e., net $N_2O$ reduction) within the same soil chamber and at two extremes of the measured soil moisture, during the early wet spring of 2015 and during the driest period of the 2016 growing season (see Figure 2c,h and red circles in Figure 3f).

In general, there was little bias in the relations between the observed and simulated GHG fluxes (slope ranged between 0.98 and 1.10; Figure 4). The 95% CI of the simulated GHGs for all, $CO_2$, $CH_4$, and $N_2O$, were narrow and the model parameter values were generally well constrained. The interquartile ranges in the posterior distributions of all parameters were less than half of their respective prior interquartile ranges (Table 1). The prior interquartile ranges

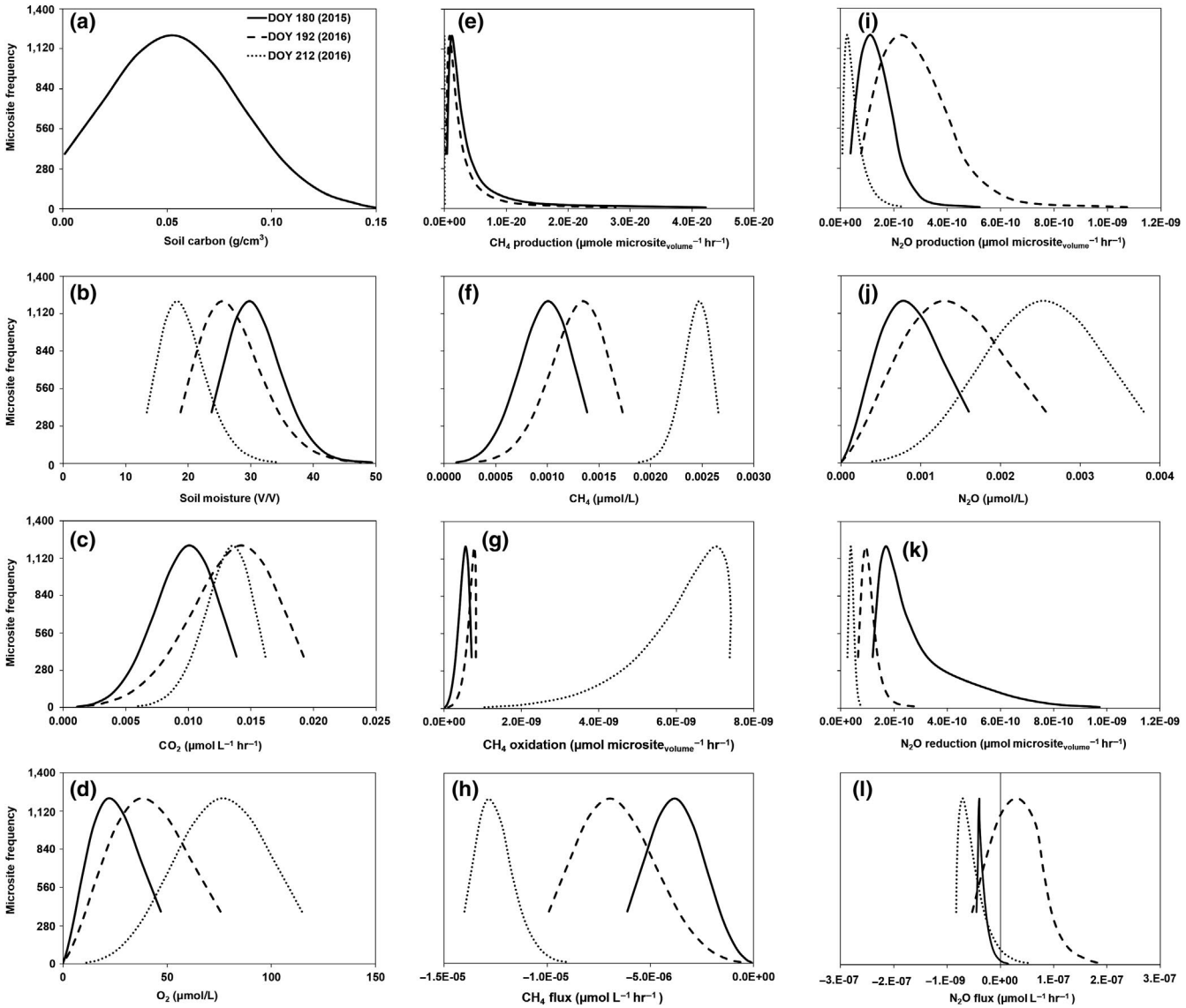


**FIGURE 5** Microsite probability distribution functions (PDFs) of soil carbon (a), soil moisture (b), $CO_2$ flux (c), $O_2$ concentration (d), $CH_4$ production (e), $CH_4$ concentration (f), $CH_4$ oxidation (g), $CH_4$ flux (h), $N_2O$ production (i), $N_2O$ concentration (j), $N_2O$ reduction (k), and $N_2O$ flux (l). Solid, dashed, and dotted lines represent simulated microsite PDFs of individual processes for DOY 180, 2015 (SoilM = 32.6 v/v and SoilT = 12.0°C); DOY 192, 2016 (SoilM = 25.4 v/v and SoilT = 13.8°C); and DOY 212, 2016 (SoilM = 18.2 v/v and SoilT = 16.3°C), respectively, and correspond to three scenarios presented in the discussion section. DOY, day of year; SoilM, soil moisture; SoilT, soil temperature

represent the approximate upper and lower bounds of the measured values from the relevant literature.

The effective depth in the DAMM-GHG model was optimized to a median value of 7 cm (min–max range: 6–11 cm; Table 1), indicating that most of the important processes affecting the net GHG fluxes that we measured with chambers were occurring within the topsoil horizons at this site. The number of microsites within the 0.07 $m^2$ chamber footprint was optimized to a median value of 7,000 (min–max range: 2,000–9,000; Table 1), indicating that the simulated microsites were about 3.6 mm in diameter, which could include macroaggregates and clusters of fine roots and pockets of organic debris.

## 3.3 | Sensitivity analysis

Soil moisture primarily (and soil temperature secondarily) controlled the microsite PDFs of production, consumption, and diffusion processes of $CO_2$, $CH_4$, and $N_2O$. The net flux is the net effect of production, consumption, and diffusion of individual gases (Figure 5; Figure S10). Of all parameters, the most sensitive ones were those that control the $V_{max}$ terms in the Arrhenius equation ($E_a$ and $\alpha$) for production and consumption of individual GHGs, followed by the half-saturation constants (*k*Ms) and $O_2$ inhibition coefficients (*k*Is) for each process (Figure 6). The linear dependence of the DAMM-GHG model parameters was generally low and was usually below the threshold of 15 (with a few exceptions) identified for potential equifinality issues (Figure 7).

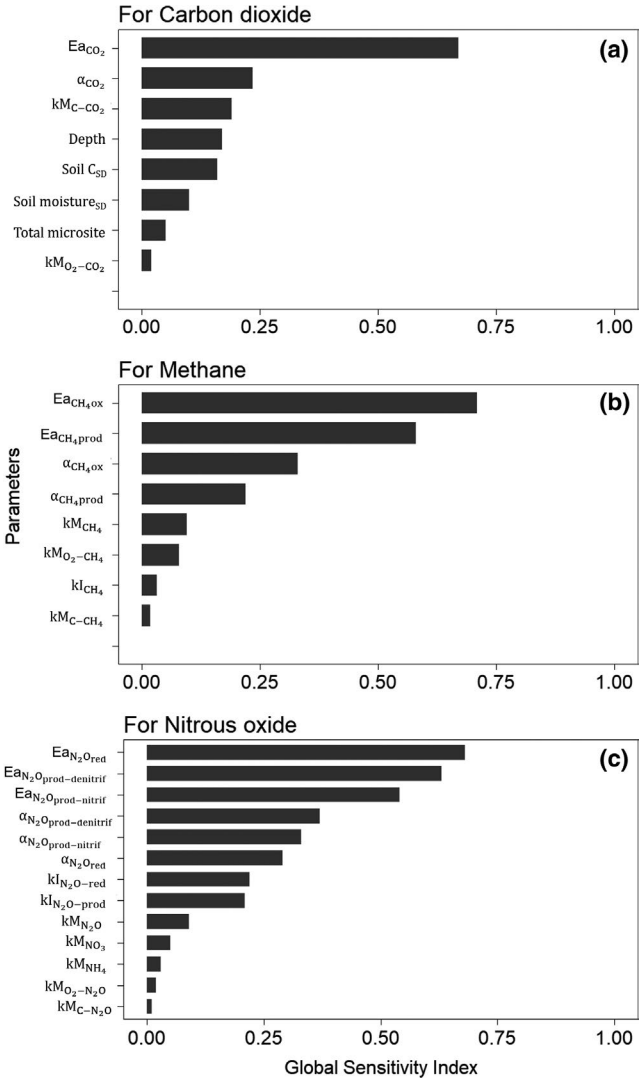


**FIGURE 6** Sensitivity indices of the DAMM-GHG model parameters for $CO_2$ (a), $CH_4$ (b), and $N_2O$ (c) modules, respectively

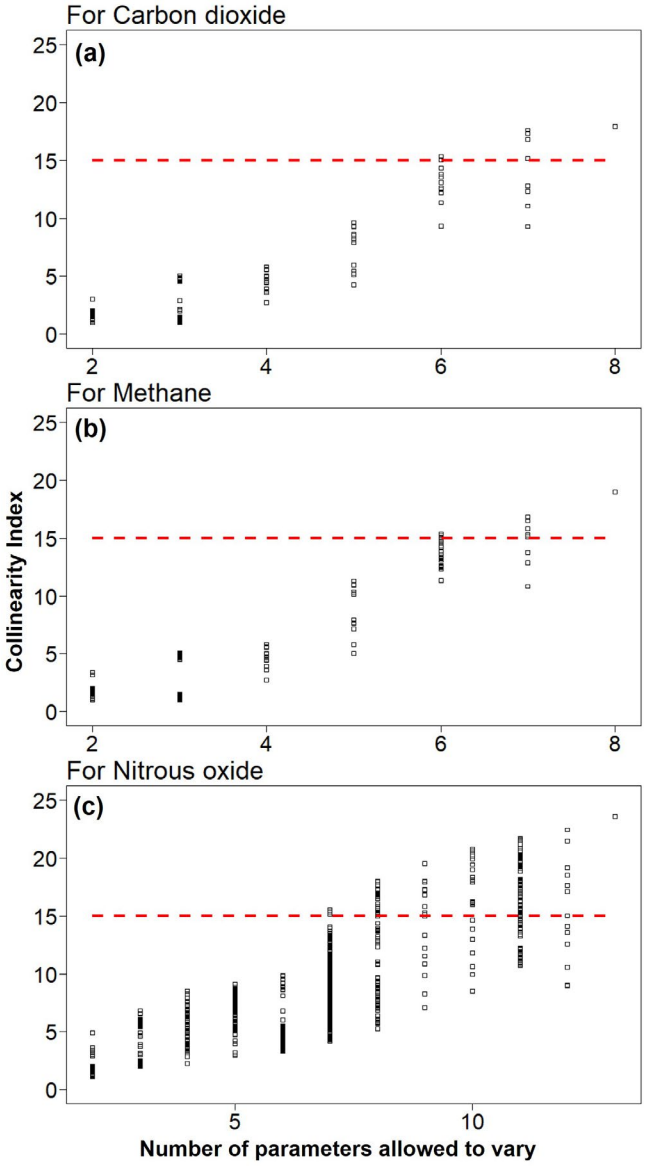


**FIGURE 7** Collinearity indices of the DAMM-GHG model parameters for $CO_2$ (a), $CH_4$ (b), and $N_2O$ (c) modules, respectively. Each point represents a unique combination of parameters allowed to vary while others are held constant. Dashed horizontal lines represent threshold value above which approximate linear dependence of model parameters increases and poor identifiability can be expected (Omlin, 1993)

## 4 | DISCUSSION

Our goal is a novel integration of measurement and modeling of three key greenhouse gases to improve understanding of and modeling capacity for interactions of belowground temperature, moisture, and substrate supply that control the net soil emissions of $CO_2$, $CH_4$, and $N_2O$. To this end, we built upon the DAMM model, which mechanistically simulates soil Rh using Arrhenius equations, diffusion functions, and Michaelis–Menten enzyme kinetics (Davidson et al., 2012, 2014). Our framework of the DAMM-GHG model is unique in that it represents the simultaneous production and consumption of all three GHGs within the same soil biophysical framework using microsite PDFs. Below we discuss the performance of the DAMM-GHG model and the utility of the microsite PDFs in reproducing the spatial and temporal dynamics of observed $CO_2$, $CH_4$, and $N_2O$ fluxes within a multiple constraint framework.

### 4.1 | Microsite representation captures co-occurrence of methane oxidation and nitrous oxide reduction

Consumption of atmospheric $N_2O$ via classical denitrification should occur only under reducing conditions. Yet, we have observed net uptake of atmospheric $CH_4$ (oxidation) and uptake of atmospheric $N_2O$ (reduction) simultaneously in well-drained soils of Howland forest under both low and high soil moisture levels. With the advent of high frequency and high sensitivity flux measurement technology, we can be confident that these modest uptake rates of both $CH_4$ and $N_2O$ are significantly different from zero and are not measurement errors or artifacts (Figures 2 and 4; also see Figure S4). These seemingly contradictory observations have been qualitatively explained by describing diffusional constraints of gas transport as follows: both $CH_4$ and $N_2O$ can diffuse into well-drained soils; the $CH_4$ is oxidized at microsites where $O_2$ is abundant; while $N_2O$ is reduced at other microsites where $N_2O$ is present and Rh is sufficiently rapid to consume $O_2$. Here, we demonstrate that this qualitative explanation can be expressed in a mathematically consistent biophysical process model that is numerically consistent with simultaneously measured fluxes of these gases.

The area under a soil chamber was partitioned according to a bivariate log-normal PDF of soil C and moisture across a range of microsites, which leads to a PDF of $CO_2$ production and $O_2$ consumption among microsites. The resulting broad range of microsite $O_2$ concentrations determines the PDF of microsites that produce or consume $CH_4$ and $N_2O$ according to Michaelis–Menten and Arrhenius functions for each process (Figure 1; Figure S1). Concentrations of below ambient $N_2O$ (hot spots of $N_2O$ reduction) occur in microsites with simulated high C and high moisture. Net consumption and production of $CH_4$ and $N_2O$ are simulated within a chamber as the average of all soil microsite simulations. To demonstrate that it is numerically feasible for microsites of $N_2O$ reduction and $CH_4$ oxidation to co-occur under a single chamber, we discuss three different scenarios where mean soil moisture levels cover the envelope of observed soil moisture in our study area (Figure 5).

Of the two growing seasons, we measured highest bulk soil moisture (32.6 v/v) on June 29 (DOY 180), 2015. Consequently, microsite PDFs of soil moisture ranged from 23.7 v/v to as high as 47.7 v/v (solid line in Figure 5b). Microsites with high soil moisture limited diffusion of gaseous $O_2$ through air-filled pore space. Simultaneously, soils had warmed up enough during the late spring of 2015 for soil respiration to exceed 100 mg $CO_2$-C $m^{-2}$ $hr^{-1}$, which created significant $O_2$ demand in microsites with high soil C. Relatively high soil respiration along with limited $O_2$ diffusion resulted in a large fraction of total soil microsites with low $O_2$ concentrations (solid line in Figure 5d). Production of $N_2O$ was high in microsites with high soil C. However, reducing environments favored $N_2O$ reduction more than $N_2O$ production in microsites with low $O_2$ concentrations. Together, the PDFs of soil microsites resulted in a modest net negative mean flux of $N_2O$ (solid line in Figure 5l). Classical theories of biological denitrification processes fit with our observations of net negative fluxes of $N_2O$ under conditions of high soil moisture (and soil C) when enzymatic reduction of $N_2O$ to $N_2$ under reducing environment outcompete $N_2O$ production rates, especially in nitrogen-limited systems like our field site (Davidson, Keller, Erickson, Verchot, & Veldkamp, 2000; Davidson et al., 1993; Firestone & Davidson, 1989). Although $N_2O$ reduction slightly exceeded $N_2O$ production under these conditions, net uptake rates of atmospheric $N_2O$ were low, because diffusion of atmospheric $N_2O$ into the soil, while occurring and thus supporting some uptake, was also limited by high water-filled pore space.

The diffusion of atmospheric $N_2O$ into the soil increased during the drier 2016 summer, thus enabling somewhat larger net uptake of atmospheric $N_2O$. The observed soil moisture content of 18.2 v/v on July 30 (DOY 212), 2016, approximately represents the first quantile of observed soil moisture across 2015 and 2016 growing seasons. Rates of $N_2O$ production during nitrification and denitrification were low in a large majority of microsites due to the oxygen inhibition effects as well as the diffusional constraints of soil C, ammonium, and nitrate substrates at low soil moisture. However, greater diffusion of atmospheric $N_2O$ to soil microsites also increased the microsite concentrations of $N_2O$ (dotted line in Figure 5j), including a small fraction of microsites with sufficiently low $O_2$ concentrations to not fully inhibit $N_2O$ reduction (i.e., the simulated $O_2$ was near the *k*I for $N_2O$ reduction ($kI_{N_2O\text{- red}}$) in approximately 10% of total microsites, resulting in net negative flux of $N_2O$ (dotted line in Figure 5d; Table 1). Our observation of a net soil sink of atmospheric $N_2O$ during summer drying events match with reports from other natural and managed ecosystems, ranging from tropical to temperate climates, where net uptake of atmospheric $N_2O$ has been measured when mean bulk soil moisture was drier than would normally be expected for $N_2O$ reduction (Donoso, Santana, & Sanhueza, 1993; Flechard, Neftel, Jocher, Ammann, & Fuhrer, 2005; Goldberg & Gebauer, 2009; Verchot et al., 2000; Yamulki, Goulding, Webster, & Harrison, 1995). In this case, however, we can demonstrate quantitatively that reducing

conditions in only about 10% of the microsites was sufficient to enable net uptake of atmospheric $N_2O$.

In contrast to the above two examples, intermediate soil moisture conditions are favorable for production to exceed consumption, resulting in modest net emissions of $N_2O$ from soil to the atmosphere. Within this context, observed soil moisture content of 25.4 v/v on July 10, 2016 (DOY 192; dashed lines in Figure 5), approximately represents the third quantile of observed soil moisture across 2015 and 2016 growing seasons (Figure 5b). As expected, $N_2O$ production was greatest at this intermediate soil moisture (Figure 5j), especially in microsites with high soil C. Because $N_2O$ production was much higher than the very low $N_2O$ reduction rates (Figure 5k) in a sufficiently large number of total soil microsites, a net positive mean $N_2O$ flux resulted (Figure 5l).

Previous studies indicated that $N_2O$ production during biological nitrification and denitrification often peak at 50%–80% of water-filled pore space (Davidson, 1991; Metivier, Pattey, & Grant, 2009), when soil moisture may be sufficiently high such that nitrate and nitrite are more available than $O_2$ as the alternate elector acceptor in many microsites, but the soil $O_2$ content is still high enough to mostly inhibit the reduction of $N_2O$ to $N_2$. This is the basis of the soil moisture function of the conceptual hole-in-the-pipe model (Firestone & Davidson, 1989). This relationship between soil moisture and $N_2O$ production is often represented in models as an empirical statistical algorithm, such as a polynomial or similar function (e.g., Del Grosso et al., 2001; Potter, Matson, Vitousek, & Davidson, 1996). In contrast, the responses to soil moisture in the DAMM-GHG model produce the response pattern across simulated microsites (Figure S7) predicted by the conceptual hole-in-the-pipe model as an emergent property of the role of $O_2$ as substrate (for nitrification, see Figure S1) or inhibitor, as represented by different $k$I values ($kI_{N_2O\text{-}prod}$ and $kI_{N_2O\text{-}red}$) used in DAMM mechanistic functions (Table 1).

For $CH_4$, the microsite PDFs of production, consumption, and net emission were relatively straightforward. Methane production was high in a relatively few numbers of microsites with high soil moisture (and soil C). In contrast, $CH_4$ oxidation was high in the majority of microsites, which had low soil moisture, as the diffusion of both substrates ($O_2$ and $CH_4$) increased with decreasing soil moisture. Note that $CH_4$ production was several orders of magnitude lower than $CH_4$ oxidation across the simulated range of microsite moisture contents in our study, mainly due to significant oxygen inhibition. Therefore, microsite PDFs of $CH_4$ oxidation primarily dominated the net $CH_4$ emission, where net $CH_4$ emission linearly decreased with decreasing soil moisture (Figure 5e–h).

Taken together, these results demonstrate that representing production, consumption, and diffusion processes as a function of soil microsite PDFs can neatly encapsulate the factors affecting emissions of $CO_2$, $CH_4$, and $N_2O$ in field studies and their underlying mechanisms. We also did a comparison of the model performance to a conventional framework, where we kept identical soil C and soil moisture values, set to the average values observed for the bulk soil, across all microsites. Although the performance of the model without microsite PDF was comparable to the one with microsite PDF for $CO_2$, model performance for $CH_4$ and $N_2O$ was strongly affected by microsite variability (Figures S8 and S9). The model without microsite PDF simulated less uptake of $CH_4$ overall, had larger than observed peaks and valleys during in wet-up and dry-down events, and had more biased residuals (Figures S8b,g and S9b,e). For $N_2O$, the model with PDF representation of microsite variation also had an overall better fit to the observations and less biased residuals (Figures S8c,h and S9c,f).

The model–data fusion algorithm we used tends to reduce the overall model–data mismatch for the entire measurement window, and so it is not surprising that there are periods within that window where simulations do not match observations as well, such as the $CO_2$ and $CH_4$ fluxes of spring 2016 (Figure 2). This may also be due to other factors not included in the DAMM-GHG model, such as impacts of spring freeze–thaw cycles on C availability or phenology of root exudates. Additionally, the lower fraction of observed variability of $N_2O$ fluxes accounted for by the model, compared to $CO_2$ and $CH_4$ fluxes, can be attributed to: (a) the low signal-to-noise ratio inherent to very low $N_2O$ fluxes; and (b) the increased number and complexity of interactions of substrates (and inhibitors) for production (e.g., C, $O_2$, $NH_4^+$, and $NO_3^-$) and consumption (e.g., C, $O_2$, and $N_2O$) of $N_2O$ during nitrification and denitrification that are represented numerically in the model with additional parameters (Figures 2 and 4). We further discussed how these potential interacting processes might have increased the covariation of parameters related to $N_2O$ dynamics than those related to $CO_2$ and $CH_4$ dynamics (see Section 4.3).

## 4.2 | Sensitivity analysis

### 4.2.1 | Sensitivity of predicted greenhouse gas fluxes to model parameters

Sensitivity indices indicated that the parameters representing the $V_{max}$ terms in the Arrhenius equation ($\alpha$ and $E_a$) for production and consumption of each gas were the most influential for all three GHGs (Figure 6a–c), which is in line with other reports (Abramoff, Davidson, & Finzi, 2017; Zarnetske, Haggerty, Wondzell, Bokil, & González-Pinzón, 2012). Sensitivity of GHG fluxes to the parameters representing Michaelis–Menten equations was secondary to those of the $\alpha$(s) and $E_a$(s), where the individual ranking was associated with the importance of controlling drivers. Following $\alpha$(s) and $E_a$(s), some of the half-saturation constants, that is, $k$M(s), were more important than others. For example, relatively higher sensitivity indices of the half-saturation constants of $CH_4$ ($kM_{CH_4}$) and $O_2$ ($kM_{O_2\text{-}CH_4}$) for $CH_4$ oxidation as compared to the half-saturation constants of C ($kM_{C\text{-}CH_4}$) and inhibition coefficient of $O_2$ ($kI_{CH_4}$) for $CH_4$ production can be explained by the dominant role of $CH_4$ oxidation in controlling net $CH_4$ emissions in our study. The inhibition coefficients of $O_2$ for $N_2O$ reduction ($kI_{N_2O\text{-}red}$) and $N_2O$ production ($kI_{N_2O\text{-}prod}$), along with the half-saturation constant of $N_2O$ for $N_2O$ reduction ($kM_{N_2O}$), had relatively higher sensitivity indices than those for the half-saturation constant of ammonium ($kM_{NH_4}$) and $O_2$ ($kM_{O_2\text{-}N_2O}$) during nitrification and nitrate ($kM_{NO_3}$) and C $kM_{C\text{-}N_2O}$ during denitrification,

respectively. These results indicate the greater importance of reducing conditions and the diffusive supply of $N_2O$ in controlling net $N_2O$ emission at our site than either the concentrations of $NH_4^+$ and $O_2$ substrates for nitrification or $NO_3^-$ and C substrates for denitrification. This result may be particular to our site where $NO_3^-$ is uniformly low and the seasonal trend of $NH_4^+$ is much less dynamic than that of soil moisture (Fernandez et al., 1995). We speculate that $kM_{NH_4}$ and $kM_{NO_3}$ might be more commonly important in agricultural soils, where large temporal variations in $NH_4^+$ and $NO_3^-$ are expected depending on the timing of fertilization and crop uptake.

### 4.2.2 | Sensitivity of predicted greenhouse gas fluxes to model drivers

Soil moisture primarily (and soil temperature secondarily) controlled the skewness of the microsite PDFs of production, consumption, and diffusion processes of each gas (Figure S10). Within this context, it is important to note that even though the parameters representing the $V_{max}$ terms in the Arrhenius equation ($E_a$ and $\alpha$) had higher sensitivity indices than the Michaelis–Menten parameters that represent the influence of soil moisture (Figure 6a–c), most of the temporal variations in $CH_4$ and $N_2O$ fluxes were nevertheless explained by soil moisture rather than temperature. The correlation matrix in Figure S5 also indicates that soil moisture, rather than soil temperature, controlled the temporal variation of $CH_4$ and $N_2O$ fluxes. In other words, if the $E_a$ value is changed, the average simulated flux for the entire time period increases or decreases significantly, but the within-season variation in $CH_4$ and $N_2O$ fluxes is still dominantly influenced by variation in soil moisture (Figures S6 and S10).

## 4.3 | Collinearity analysis

As expected, the CI increases as the number of variable parameters increases (Figure 7). Given the parsimonious model structure, we had few problems of identifiability of the processes for $CO_2$ and $CH_4$ module, and the most parameter combinations remain below the threshold value of 15 (Brun, Kühni, Siegrist, Gujer, & Reichert, 2002; Omlin et al., 2001). However, we do have some parameter combinations with CI > 15 for the $N_2O$ module, due to probable ambiguity of whether $N_2O$ fluxes are affected more by production via nitrification (affected by $NH_4^+$ substrate), production via denitrification (affected by $NO_3^-$ substrates), or consumption of $N_2O$ (affected by $N_2O$ diffusion). Trade-offs of processes within models can account for inflation of CI values (Keenan, Carbone, Reichstein, & Richardson, 2011; Richardson et al., 2010), which is likely the case for the $N_2O$ module relative to the $CO_2$ and $CH_4$ modules. Overall, however, collinearity analysis indicates that the chances of having equifinality issues characterized by biologically improbable process representations were generally low in the DAMM-GHG model.

We believe that this success is largely due to the multiple constraints imposed by simultaneously modeling data streams of three different gases, which enabled us to capture the influence of temporally and spatially varying drivers on GHG fluxes (Myrgiotis, Williams, Topp, & Rees, 2018). For example, when simulating only $CH_4$ flux, a better fit of the model to the data might be achieved by adjusting either the Michaelis–Menten parameters or the diffusion parameters, but it may be impossible to know which the "correct" adjustment is. However, if $N_2O$ and $CO_2$ are also being simultaneously simulated, then adjusting the diffusion parameters will affect simulations of all three gases, whereas adjusting the Michaelis–Menten parameters for $CH_4$ oxidation should have little effect on the other two gases. Hence, the additional constraints help identify which model parameterizations are consistent with all three data streams of flux measurements.

## 4.4 | Microsite probability distribution functions permit model parsimony

Simulating a 3-D array of soil aggregates or pore networks (Arah & Vinten, 1995; Ebrahimi & Or, 2014; Yan et al., 2016) is another approach for representing spatial heterogeneity of soil matrix in biogeochemical models. However, explicit representation of soil spatial variability requires detailed information on soil structure, involving high-throughput instrumentations such as X-ray CT scan (see Carducci, Zinn, Rossoni, Heck, & Oliveira, 2017) and may require greater computational power than our PDF approach. Because of the limited measurements on the spatial variability of soil aggregates (or pores) at a plot scale, let alone at larger scales, and because of the increased computational complexity in spatially explicit model structures, scaling up of 3-D soil aggregate (or pore network) models to the ecosystem models and ESMs is still challenging.

Statistically representing microsite variation as PDFs in the DAMM-GHG model offers a relatively computationally efficient, yet mechanistically consistent, alternative way of simulating soil heterogeneity and maintaining model parsimony, as in the original DAMM model (Davidson et al., 2012, 2014; Sihi et al., 2018). We believe that our framework could be used to simulate fluxes of GHGs from other natural and managed systems as well as be scaled up to ecosystem models and ESMs.

## 4.5 | Opportunities for future improvement of the DAMM-GHG model

We represented all microsite-scale processes by optimizing an equivalent depth for Rh, where most of the biological reactions appear to happen in the soil of this study site (posterior range: 6–11 cm) and fixed that depth for simulating processes related to production and consumption of $CH_4$ and $N_2O$. This simplification allowed us to use unitless diffusion constants for gaseous and dissolved substrates and to avoid needing to know exact diffusion path lengths (see Davidson et al., 2012 for details). Exploring heterogeneity of diffusivity within and among soil horizons could be an appropriate next step.

Including more complex models of gas diffusion that includes variable diffusivity between intra-aggregate and inter-aggregate

pore spaces may be more appropriate for aggregated media like soil (Millington & Shearer, 1971; Resurreccion et al., 2010). Representing soil microsite PDFs in more than one vertically stratified soil horizon by differentiating between the organic and various mineral horizons may be needed for application to other sites (e.g., wetland with a seasonally variable depth to the water table), such that transport of gases between soil horizons and across soil–air boundary can be estimated using Fick's law. Measured vertical concentration profiles of soil gases could serve as additional data constraints for soil gas concentration profiles that become emergent simulated properties of this modeling approach. It would also be useful to have a data stream of heterogeneity of $O_2$ or redox potentials across microsites, but that would require new generations of microprobes.

Additionally, techniques that disentangle gross production and gross consumption rates of $CH_4$ and $N_2O$ under field conditions could increase the predictive power of the dynamics of soil GHGs fluxes. For example, Chanton, Powelson, Abichou, and Hater (2008) reported that measuring stable carbon isotope of emitted $CH_4$ ($^{13}CH_4$) is a feasible way to quantify gross $CH_4$ oxidation in situ. Likewise, Wen et al. (2016) demonstrated that $^{15}N_2O$ pool dilution method can be effective to measure atmospheric $N_2O$ uptake in soil under field conditions. In situ quantification of microbial activities pertaining to gross production and consumption of $CH_4$ and $N_2O$ can also be pursued following the gas push-pull method (Urmann, Gonzalez-Gil, Schroth, Hofer, & Zeyer, 2005). Quantifying gross nitrogen transformations using stable isotope tracing could help constrain the sources of $N_2O$ emissions (Morse & Bernhardt, 2013; Müller, Rütting, Kattge, Laughlin, & Stevens, 2007; Myrold & Tiedje, 1986).

In addition to nitrification and biological denitrification, other bacterial (Jensen & Burris, 1986; Yamazaki, Yoshida, Wada, & Matsuo, 1987) and fungal (Hayatsu, Tago, & Saito, 2008; Shoun, Kim, Uchiyama, & Sugiyama, 1992) contributions, as well as abiotic (Davidson, Chorover, & Dail, 2003; Vieten, 2008) sinks of $N_2O$ in soil could be explored if warranted. Adding other controlling factors, such as pH effects, temporal dynamics of enzyme synthesis, and root exudation, could improve model performance for some sites (Butterbach-Bahl et al., 2013; Zheng & Doskey, 2015). In all of these cases, however, the potential additional explanatory value of more parameters and model complexity must be balanced with the availability of data to constrain them and with the advantages of model structure parsimony.

## 5 | CONCLUSIONS

Representing microsite heterogeneity as PDFs related to predictive processes offers a new approach for numerical representation of methanogenesis, methane oxidation, nitrification, and denitrification and other spatially and temporally variable microbial processes in soil. Our ability to accurately measure and skillfully model rates of these processes has been hampered by highly variable soil microsite conditions, which are difficult to measure and simulate, but our use of PDFs to represent that variability offers a promising and computationally efficient approach. In addition, by measuring and modeling all three greenhouse gases ($CO_2$, $CH_4$, and $N_2O$), we have mechanistically and quantitatively explained the apparent paradox of observed simultaneous aerobic respiration that produces $CO_2$, $CH_4$ uptake (oxidation), $CH_4$ production, and $N_2O$ uptake (reduction) in the same soil profile. Skillful representations of multiple ecologically relevant processes increase confidence of getting the right answers for the right reasons. This relatively parsimonious process modeling framework has the potential to be implemented within ecosystem models and ESMs to better capture the dynamics of soil-based greenhouse gases at landscape, regional, and global scales.

## ACKNOWLEDGEMENTS

This work was supported by the USDA NIFA award # 2014-67003-22073. Research activities at the Howland Forest are supported by the USDA Forest Service's Northern Research Station and the US Department of Energy's BER (Office of Science) Program. We thank Dr. Andrew D. Richardson for facilitating our access to the Odyssey cluster supported by the FAS Division of Science at the Harvard University, which we used for computational purposes. All data used in this paper are available through Richardson et al. (2019). R scripts used for this modeling work are made available as a GitHub repository (https://github.com/dsihi/DAMM-GHG).

## ORCID

*Debjani Sihi* https://orcid.org/0000-0002-5513-8862
*Eric A. Davidson* https://orcid.org/0000-0002-8525-8697
*Kathleen E. Savage* https://orcid.org/0000-0002-1649-5314

## REFERENCES

Abramoff, R. Z., Davidson, E. A., & Finzi, A. C. (2017). A parsimonious modular approach to building a mechanistic belowground carbon and nitrogen model. *Journal of Geophysical Research: Biogeosciences*, *122*(9), 2418–2434. https://doi.org/10.1002/2017JG003796

Abramoff, R., Xu, X., Hartman, M., O'Brien, S., Feng, W., Davidson, E., … Mayes, M. A. (2018). The Millennial model: In search of measurable pools and transformations for modeling soil carbon in the new century. *Biogeochemistry*, *137*(1), 51–71. https://doi.org/10.1007/s10533-017-0409-7

Angert, A., Yakir, D., Rodeghiero, M., Preisler, Y., Davidson, E. A., & Weiner, T. (2015). Using $O_2$ to study the relationships between soil $CO_2$ efflux and soil respiration. *Biogeosciences*, *12*, 2089–2099. https://doi.org/10.5194/bg-12-2089-2015

Arah, J. R. M., & Stephen, K. D. (1998). A model of the processes leading to methane emission from peatland. *Atmospheric Environment*, *32*(19), 3257–3264. https://doi.org/10.1016/S1352-2310(98)00052-1

Arah, J. R. M., & Vinten, A. J. A. (1995). Simplified models of anoxia and denitrification in aggregated and simple-structured soils. *European Journal of Soil Science*, *46*(4), 507–517. https://doi.org/10.1111/j.1365-2389.1995.tb01347.x

Arrhenius, S. (1889). Über die Reaktionsgeschwindigkeit bei der Inversion von Rohrzucker durch Säuren. *Zeitschrift für Physikalische Chemie*, *4U*(1), 226. https://doi.org/10.1515/zpch-1889-0416

Bernhardt, E. S., Blaszczak, J. R., Ficken, C. D., Fork, M. L., Kaiser, K. E., & Seybold, E. C. (2017). Control points in ecosystems: Moving beyond the hot spot hot moment concept. *Ecosystems*, *20*(4), 665–682. https://doi.org/10.1007/s10021-016-0103-y

Bidot, C., Lamboni, M., & Monod, H. (2018). _multisensi: Multivariate Sensitivity Analysis_. R package version 2.1-1. Retrieved from https://CRAN.R-project.org/package=multisensi

Bodelier, P., Libochant, J. A., Blom, C., & Laanbroek, H. J. (1996). Dynamics of nitrification and denitrification in root-oxygenated sediments and adaptation of ammonia-oxidizing bacteria to low-oxygen or anoxic habitats. *Applied and Environment Microbiology*, *62*(11), 4100–4107.

Brewer, P., Calderón, F., Vigil, M., & von Fischer, J. (2018). Impacts of moisture, soil respiration, and agricultural practices on methanogenesis in upland soils as measured with stable isotope pool dilution. *Soil Biology and Biochemistry*, *127*, 239–251. https://doi.org/10.1016/j.soilbio.2018.09.014

Brun, R., Kühni, M., Siegrist, H., Gujer, W., & Reichert, P. (2002). Practical identifiability of ASM2d parameters—Systematic selection and tuning of parameter subsets. *Water Research*, *36*(16), 4113–4127. https://doi.org/10.1016/S0043-1354(02)00104-5

Brun, R., Reichert, P., & Künsch, H. R. (2001). Practical identifiability analysis of large environmental simulation models. *Water Resources Research*, *37*(4), 1015–1030. https://doi.org/10.1029/2000WR900350

Butterbach-Bahl, K., Baggs, E. M., Dannenmann, M., Kiese, R., & Zechmeister-Boltenstern, S. (2013). Nitrous oxide emissions from soils: How well do we understand the processes and their controls? *Philosophical Transactions of the Royal Society B: Biological Sciences*, *368*(1621), 20130122. https://doi.org/10.1098/rstb.2013.0122

Canion, A., Kostka, J. E., Gihring, T. M., Huettel, M., van Beusekom, J. E. E., Gao, H., … Kuypers, M. M. M. (2014). Temperature response of denitrification and anammox reveals the adaptation of microbial communities to in situ temperatures in permeable marine sediments that span 50° in latitude. *Biogeosciences*, *11*(2), 309–320. https://doi.org/10.5194/bg-11-309-2014

Carbone, M. S., Richardson, A. D., Chen, M., Davidson, E. A., Hughes, H., Savage, K. E., & Hollinger, D. Y. (2016). Constrained partitioning of autotrophic and heterotrophic respiration reduces model uncertainties of forest ecosystem carbon fluxes but not stocks. *Journal of Geophysical Research: Biogeosciences*, *121*(9), 2476–2492. https://doi.org/10.1002/2016JG003386

Carducci, C. E., Zinn, Y. L., Rossoni, D. F., Heck, R. J., & Oliveira, G. C. (2017). Visual analysis and X-ray computed tomography for assessing the spatial variability of soil structure in a cultivated Oxisol. *Soil and Tillage Research*, *173*, 15–23. https://doi.org/10.1016/j.still.2016.03.006

Cattânio, J. H., Davidson, E. A., Nepstad, D. C., Verchot, L. V., & Ackerman, I. L. (2002). Unexpected results of a pilot throughfall exclusion experiment on soil emissions of $CO_2$, $CH_4$, $N_2O$, and NO in eastern Amazonia. *Biology and Fertility of Soils*, *36*(2), 102–108. https://doi.org/10.1007/s00374-002-0517-x

Chanton, J. P., Powelson, D. K., Abichou, T., & Hater, G. (2008). Improved field methods to quantify methane oxidation in landfill cover materials using stable carbon isotopes. *Environmental Science & Technology*, *42*(3), 665–670. https://doi.org/10.1021/es0710757

Chapuis-Lardy, L., Wrage, N., Metay, A.,Chotte, J. L., & Bernoux, M. (2007). Soils, a sink for $N_2O$? A review. *Global Change Biology*, *13*(1), 1–17. https://doi.org/10.1111/j.1365-2486.2006.01280.x

Ciais, P., Sabine, C., Bala, G., Bopp, L., Brovkin, V., Canadell, J., … Heimann, M. (2014). Carbon and other biogeochemical cycles. In T. F. Stocker, D. Qin, G.-K. Plattner, M. Tignor, S. K. Allen, J. Boschung, … P. M. Midgley (Eds.), *Climate change 2013: The physical science basis. Contribution of Working Group I to the Fifth Assessment Report of the Intergovernmental Panel on Climate Change* (pp. 465–570). Cambridge, UK: Cambridge University Press.

Conrad, R. (1996). Soil microorganisms as controllers of atmospheric trace gases ($H_2$, CO, $CH_4$, OCS, $N_2O$, and NO). *Microbiological Reviews*, *60*(4), 609–640.

Conrad, R. (2009). The global methane cycle: Recent advances in understanding the microbial processes involved. *Environmental Microbiology Reports*, *1*(5), 285–292. https://doi.org/10.1111/j.1758-2229.2009.00038.x

Crill, P., Martikainen, P., Nykanen, H., & Silvola, J. (1994). Temperature and N fertilization effects on methane oxidation in a drained peatland soil. *Soil Biology and Biochemistry*, *26*(10), 1331–1339. https://doi.org/10.1016/0038-0717(94)90214-3

Davidson, E. A. (1991). Fluxes of nitrous oxide and nitric oxide from terrestrial ecosystems. In J. E. Rogers & W. B. Whitman (Eds.), *Microbial production and consumption of greenhouse gases: Methane, nitrous oxide, and halomethanes* (pp. 219–235). Washington, DC: American Society for Microbiology.

Davidson, E. A., Belk, E., & Boone, R. D. (1998). Soil water content and temperature as independent or confounded factors controlling soil respiration in a temperate mixed hardwood forest. *Global Change Biology*, *4*(2), 217–227. https://doi.org/10.1046/j.1365-2486.1998.00128.x

Davidson, E. A., Chorover, J., & Dail, D. B. (2003). A mechanism of abiotic immobilization of nitrate in forest ecosystems: The ferrous wheel hypothesis. *Global Change Biology*, *9*(2), 228–236. https://doi.org/10.1046/j.1365-2486.2003.00592.x

Davidson, E. A., & Janssens, I. A. (2006). Temperature sensitivity of soil carbon decomposition and feedbacks to climate change. *Nature*, *440*, 165. https://doi.org/10.1038/nature04514

Davidson, E. A., Janssens, I. A., & Luo, Y. (2006). On the variability of respiration in terrestrial ecosystems: Moving beyond Q10. *Global Change Biology*, *12*(2), 154–164. https://doi.org/10.1111/j.1365-2486.2005.01065.x

Davidson, E. A., Keller, M., Erickson, H. E., Verchot, L. V., & Veldkamp, E. (2000). Testing a conceptual model of soil emissions of nitrous and nitric oxides: Using two functions based on soil nitrogen availability and soil water content, the hole-in-the-pipe model characterizes a large fraction of the observed variation of nitric oxide and nitrous oxide emissions from soils. *BioScience*, *50*(8), 667–680. https://doi.org/10.1641/0006-3568(2000)050[0667:Tacmos]2.0.Co;2

Davidson, E. A., Matson, P. A., Vitousek, P. M., Riley, R., Dunkin, K., Garcia-Mendez, G., & Maass, J. M. (1993). Processes regulating soil emissions of NO and $N_2O$ in a seasonally dry tropical forest. *Ecology*, *74*(1), 130–139. https://doi.org/10.2307/1939508

Davidson, E. A., Samanta, S., Caramori, S. S., & Savage, K. (2012). The Dual Arrhenius and Michaelis-Menten kinetics model for decomposition of soil organic matter at hourly to seasonal time scales. *Global Change Biology*, *18*(1), 371–384. https://doi.org/10.1111/j.1365-2486.2011.02546.x

Davidson, E. A., Savage, K. E., & Finzi, A. C. (2014). A big-microsite framework for soil carbon modeling. *Global Change Biology*, *20*(12), 3610–3620. https://doi.org/10.1111/gcb.12718

Dean, J. F., Middelburg, J. J., Röckmann, T., Aerts, R., Blauw, L. G., Egger, M., … Dolman, A. J. (2018). Methane feedbacks to the global climate system in a warmer world. *Reviews of Geophysics*, *56*(1), 207–250. https://doi.org/10.1002/2017RG000559

Del Grosso, S. J., Parton, W. J., Mosier, A. R., Hartman, M. D., Keough, C. A., Peterson, G. A., … Schimel, D. S. (2001). Simulated effects of land use, soil texture, and precipitation on N gas emissions using DAYCENT. In R. F. Follett & J. L. Hatfield (Eds.), *Nitrogen in the environment: Sources, problems, and management* (pp. 413–431). Amsterdam, The Netherlands: Elsevier Science Publ.

Donoso, L., Santana, R., & Sanhueza, E. (1993). Seasonal variation of $N_2O$ fluxes at a tropical savannah site: Soil consumption of $N_2O$ during the dry season. *Geophysical Research Letters*, *20*(13), 1379–1382. https://doi.org/10.1029/93GL01537

Ebrahimi, A. N., & Or, D. (2014). Microbial dispersal in unsaturated porous media: Characteristics of motile bacterial cell motions in unsaturated

angular pore networks. *Water Resources Research*, *50*(9), 7406–7429. https://doi.org/10.1002/2014wr015897

Ebrahimi, A., & Or, D. (2018). On upscaling of soil microbial processes and biogeochemical fluxes from aggregates to landscapes. *Journal of Geophysical Research: Biogeosciences*, *123*(5), 1526–1547. https://doi.org/10.1029/2017JG004347

Eugster, W., Zeyer, K., Zeeman, M., Michna, P., Zingg, A., Buchmann, N., & Emmenegger, L. (2007). Methodical study of nitrous oxide eddy covariance measurements using quantum cascade laser spectrometery over a Swiss forest. *Biogeosciences*, *4*(5), 927–939. https://doi.org/10.5194/bg-4-927-2007

Fernandez, I. J., Lawrence, G. B., & Son, Y. (1995). Soil-solution chemistry in a low-elevation spruce-fir ecosystem, Howland, Maine. *Water, Air, and Soil Pollution*, *84*(1), 129–145. https://doi.org/10.1007/bf00479593

Fernandez, I. J., Rustad, L. E., & Lawrence, G. B. (1993). Estimating total soil mass, nutrient content, and trace metals in soils under a low elevation spruce-fir forest. *Canadian Journal of Soil Science*, *73*(3), 317–328. https://doi.org/10.4141/cjss93-034

Firestone, M. K., & Davidson, E. A. (1989). Microbiological basis of NO and $N_2O$ production and consumption in soil. In M. O. Andreae & D. S. Schimel (Eds.), *Exchange of trace gases between terrestrial ecosystems and the atmosphere* (pp. 7–21). New York, NY: John Wiley & Sons Inc.

Flechard, C. R., Neftel, A., Jocher, M., Ammann, C., & Fuhrer, J. (2005). Bi-directional soil/atmosphere $N_2O$ exchange over two mown grassland systems with contrasting management practices. *Global Change Biology*, *11*(12), 2114–2127. https://doi.org/10.1111/j.1365-2486.2005.01056.x

Goldberg, S. D., & Gebauer, G. (2009). Drought turns a Central European Norway spruce forest soil from an $N_2O$ source to a transient $N_2O$ sink. *Global Change Biology*, *15*(4), 850–860. https://doi.org/10.1111/j.1365-2486.2008.01752.x

Groffman, P. M. (2012). Terrestrial denitrification: Challenges and opportunities. *Ecological Processes*, *1*(1), 11. https://doi.org/10.1186/2192-1709-1-11

Groffman, P. M., Butterbach-Bahl, K., Fulweiler, R. W., Gold, A. J., Morse, J. L., Stander, E. K., … Vidon, P. (2009). Challenges to incorporating spatially and temporally explicit phenomena (hotspots and hot moments) in denitrification models. *Biogeochemistry*, *93*(1), 49–77. https://doi.org/10.1007/s10533-008-9277-5

Hayatsu, M., Tago, K., & Saito, M. (2008). Various players in the nitrogen cycle: Diversity and functions of the microorganisms involved in nitrification and denitrification. *Soil Science and Plant Nutrition*, *54*(1), 33–45. https://doi.org/10.1111/j.1747-0765.2007.00195.x

Holtan-Hartwig, L., Dörsch, P., & Bakken, L. R. (2002). Low temperature control of soil denitrifying communities: Kinetics of $N_2O$ production and reduction. *Soil Biology and Biochemistry*, *34*(11), 1797–1806. https://doi.org/10.1016/S0038-0717(02)00169-4

Hursh, A., Ballantyne, A., Cooper, L., Maneta, M., Kimball, J., & Watts, J. (2017). The sensitivity of soil respiration to soil temperature, moisture, and carbon supply at the global scale. *Global Change Biology*, *23*(5), 2090–2103. https://doi.org/10.1111/gcb.13489

IPCC. (2014). *Climate Change 2014: Synthesis Report. Contribution of Working Groups I, II and III to the Fifth Assessment Report of the Intergovernmental Panel on Climate Change* [Core Writing Team, R. K. Pachauri & L. A. Meyer (Eds.)]. Geneva, Switzerland: IPCC, 151 pp.

Jensen, B. B., & Burris, R. H. (1986). Nitrous oxide as a substrate and as a competitive inhibitor of nitrogenase. *Biochemistry*, *25*(5), 1083–1088. https://doi.org/10.1021/bi00353a021

Keenan, T. F., Carbone, M. S., Reichstein, M., & Richardson, A. D. (2011). The model–data fusion pitfall: Assuming certainty in an uncertain world. *Oecologia*, *167*(3), 587. https://doi.org/10.1007/s00442-011-2106-x

Keiluweit, M., Gee, K., Denney, A., & Fendorf, S. (2018). Anoxic microsites in upland soils dominantly controlled by clay content. *Soil Biology and Biochemistry*, *118*, 42–50. https://doi.org/10.1016/j.soilbio.2017.12.002

Keller, M., & Matson, P. A. (1994). Biosphere–atmosphere exchanges of trace gases in the tropics: Evaluating the effects of land use changes. In R. G. Prinn (Ed.), *Global atmospheric biospheric chemistry* (pp. 103–117). New York, NY: Plenum Press.

Körner, H., & Zumft, W. G. (1989). Expression of denitrification enzymes in response to the dissolved oxygen level and respiratory substrate in continuous culture of *Pseudomonas stutzeri*. *Applied and Environmental Microbiology*, *55*(7), 1670–1676.

Lamboni, M., Makowski, D., Lehuger, S., Gabrielle, B., & Monod, H. (2009). Multivariate global sensitivity analysis for dynamic crop models. *Field Crops Research*, *113*(3), 312–320. https://doi.org/10.1016/j.fcr.2009.06.007

Lindgren, F., & Rue, H. (2015). Bayesian spatial modelling with R-INLA. *Journal of Statistical Software*, *63*(19), 1–25. https://doi.org/10.18637/jss.v063.i19

Linn, D. M., & Doran, J. W. (1984). Effect of water-filled pore space on carbon dioxide and nitrous oxide production in tilled and nontilled soils 1. *Soil Science Society of America Journal*, *48*(6), 1267–1272. https://doi.org/10.2136/sssaj1984.03615995004800060013x

Lloyd, J., & Taylor, J. A. (1994). On the temperature dependence of soil respiration. *Functional Ecology*, *8*(3), 315–323. https://doi.org/10.2307/2389824

Lurndahl, N. (2016). *Temporal and spatial trends in the abundance of functional denitrification genes and observed soil moisture and potential denitrification rates*. MS thesis, University of Minnesota, Minneapolis.

Metivier, K. A., Pattey, E., & Grant, R. F. (2009). Using the ecosys mathematical model to simulate temporal variability of nitrous oxide emissions from a fertilized agricultural soil. *Soil Biology and Biochemistry*, *41*(12), 2370–2386. https://doi.org/10.1016/j.soilbio.2009.03.007

Millington, R. J., & Shearer, R. C. (1971). Diffusion in aggregated porous media. *Soil Science*, *111*(6), 372–378. https://doi.org/10.1097/00010694-197106000-00007

Morse, J. L., & Bernhardt, E. S. (2013). Using $^{15}N$ tracers to estimate $N_2O$ and $N_2$ emissions from nitrification and denitrification in coastal plain wetlands under contrasting land-uses. *Soil Biology and Biochemistry*, *57*, 635–643. https://doi.org/10.1016/j.soilbio.2012.07.025

Moyano, F. E., Manzoni, S., & Chenu, C. (2013). Responses of soil heterotrophic respiration to moisture availability: An exploration of processes and models. *Soil Biology and Biochemistry*, *59*, 72–85. https://doi.org/10.1016/j.soilbio.2013.01.002

Müller, C., Rütting, T., Kattge, J., Laughlin, R. J., & Stevens, R. J. (2007). Estimation of parameters in complex $^{15}N$ tracing models by Monte Carlo sampling. *Soil Biology and Biochemistry*, *39*(3), 715–726. https://doi.org/10.1016/j.soilbio.2006.09.021

Myrgiotis, V., Williams, M., Topp, C. F., & Rees, R. M. (2018). Improving model prediction of soil $N_2O$ emissions through Bayesian calibration. *Science of the Total Environment*, *624*, 1467–1477. https://doi.org/10.1016/j.scitotenv.2017.12.202

Myrold, D. D., & Tiedje, J. M. (1986). Simultaneous estimation of several nitrogen cycle rates using $^{15}N$: Theory and application. *Soil Biology and Biochemistry*, *18*(6), 559–568. https://doi.org/10.1016/0038-0717(86)90076-3

Nedwell, D. B., & Watson, A. (1995). $CH_4$ production, oxidation and emission in a U.K. ombrotrophic peat bog: Influence of $SO_4^{2-}$ From acid rain. *Soil Biology and Biochemistry*, *27*(7), 893–903. https://doi.org/10.1016/0038-0717(95)00018-A

Omlin, M., Brun, R., & Reichert, P. (2001). Biogeochemical model of Lake Zürich: Sensitivity, identifiability and uncertainty analysis. *Ecological Modelling*, *141*(1), 105–123. https://doi.org/10.1016/S0304-3800(01)00257-5

Or, D. (2019). The tyranny of small scales – on representing soil processes in global land surface models. *Water Resources Research*. https://doi.org/10.1029/2019wr024846

Parkin, T. B. (1987). Soil microsites as a source of denitrification variability. *Soil Science Society of America Journal*, *51*(5), 1194–1199. https://doi.org/10.2136/sssaj1987.03615995005100050019x

Parkin, T. B. (1993). Spatial variability of microbial processes in soil—A review. *Journal of Environmental Quality*, *22*(3), 409–417. https://doi.org/10.2134/jeq1993.00472425002200030004x

Potter, C. S., Matson, P. A., Vitousek, P. M., & Davidson, E. A. (1996). Process modeling of controls on nitrogen trace gas emissions from soils worldwide. *Journal of Geophysical Research: Atmospheres*, *101*(D1), 1361–1377. https://doi.org/10.1029/95jd02028

R Core Team. (2018). *R: A language and environment for statistical computing*. Vienna, Austria: R Foundation for Statistical Computing. Retrieved from https://www.R-project.org/

Resurreccion, A. C., Moldrup, P., Kawamoto, K., Hamamoto, S., Rolston, D. E., & Komatsu, T. (2010). Hierarchical, bimodal model for gas diffusivity in aggregated, unsaturated soils. *Soil Science Society of America Journal*, *74*(2), 481–491. https://doi.org/10.2136/sssaj2009.0055

Revolution Analytics, & Weston, S. (2015). doParallel: Foreach Parallel Adaptor for the 'parallel' Package. R package version 1.0.10. Retrieved from https://CRAN.R-918project.org/package=doParallel

Richardson, A. D., Hollinger, D. Y., Shoemaker, J. K., Hughes, H., Savage, K., & Davidson, E. A. (2019). Six years of ecosystem-atmosphere greenhouse gas fluxes measured in a sub-boreal forest. *Scientific Data*, *6*(1), 117. https://doi.org/10.1038/s41597-019-0119-1

Richardson, A. D., Williams, M., Hollinger, D. Y., Moore, D. J. P., Dail, D. B., Davidson, E. A., … Savage, K. (2010). Estimating parameters of a forest ecosystem C model with measurements of stocks and fluxes as joint constraints. *Oecologia*, *164*(1), 25–40. https://doi.org/10.1007/s00442-010-1628-y

Rue, H., Martino, S., & Chopin, N. (2009). Approximate Bayesian inference for latent Gaussian models by using integrated nested Laplace approximations. *Journal of the Royal Statistical Society: Series B (Statistical Methodology)*, *71*(2), 319–392. https://doi.org/10.1111/j.1467-9868.2008.00700.x

Saha, D., Kemanian, A. R., Montes, F., Gall, H., Adler, P. R., & Rau, B. M. (2018). Lorenz curve and gini coefficient reveal hot spots and hot moments for nitrous oxide emissions. *Journal of Geophysical Research: Biogeosciences*, *123*(1), 193–206. https://doi.org/10.1002/2017JG004041

Savage, K. E., & Davidson, E. A. (2003). A comparison of manual and automated systems for soil $CO_2$ flux measurements: Trade-offs between spatial and temporal resolution. *Journal of Experimental Botany*, *54*(384), 891–899. https://doi.org/10.1093/jxb/erg121

Savage, K. E., Davidson, E. A., Abramoff, R. Z., Finzi, A. C., & Giasson, M.-A. (2018). Partitioning soil respiration: Quantifying the artifacts of the trenching method. *Biogeochemistry*, *140*(1), 53–63. https://doi.org/10.1007/s10533-018-0472-8

Savage, K. E., Davidson, E. A., & Richardson, A. D. (2008). A conceptual and practical approach to data quality and analysis procedures for high-frequency soil respiration measurements. *Functional Ecology*, *22*(6), 1000–1007. https://doi.org/10.1111/j.1365-2435.2008.01414.x

Savage, K. E., Phillips, R., & Davidson, E. (2014). High temporal frequency measurements of greenhouse gas emissions from soils. *Biogeosciences*, *11*(10), 2709–2720. https://doi.org/10.5194/bg-11-2709-2014

Schlesinger, W. H. (2013). An estimate of the global sink for nitrous oxide in soils. *Global Change Biology*, *19*(10), 2929–2931. https://doi.org/10.1111/gcb.12239

Shoun, H., Kim, D.-H., Uchiyama, H., & Sugiyama, J. (1992). Denitrification by fungi. *FEMS Microbiology Letters*, *94*(3), 277–281. https://doi.org/10.1111/j.1574-6968.1992.tb05331.x

Sihi, D., Davidson, E. A., Chen, M., Savage, K. E., Richardson, A. D., Keenan, T. F., & Hollinger, D. Y. (2018). Merging a mechanistic enzymatic model of soil heterotrophic respiration into an ecosystem model in two AmeriFlux sites of northeastern USA. *Agricultural and Forest Meteorology*, *252*, 155–166. https://doi.org/10.1016/j.agrformet.2018.01.026

Silver, W. L., Lugo, A. E., & Keller, M. (1999). Soil oxygen availability and biogeochemistry along rainfall and topographic gradients in upland wet tropical forest soils. *Biogeochemistry*, *44*(3), 301–328. https://doi.org/10.1007/bf00996995

Soetaert, K. (2016). R Package FME: Inverse modelling, sensitivity. Monte Carlo—Applied to a dynamic simulation model (CRAN Vignette 2). Retrieved from https://cran.r-project.org/web/packages/FME/vignettes/FMEdyna.pdf

Soetaert, K., & Petzoldt, T. (2010). Inverse modelling, sensitivity and Monte Carlo analysis in R using package FME. *Journal of Statistical Software*, *33*(3), 1–28.

Stark, J. M. (1996). Modeling the temperature response of nitrification. *Biogeochemistry*, *35*(3), 433–445. https://doi.org/10.1007/BF02183035

Stark, J. M., & Firestone, M. K. (1996). Kinetic characteristics of ammonium-oxidizer communities in a California oak woodland-annual grassland. *Soil Biology and Biochemistry*, *28*(10–11), 1307–1317. https://doi.org/10.1016/S0038-0717(96)00133-2

Stoyan, H., De-Polli, H., Böhm, S., Robertson, G. P., & Paul, E. A. (2000). Spatial heterogeneity of soil respiration and related properties at the plant scale. *Plant and Soil*, *222*(1), 203–214. https://doi.org/10.1023/a:1004757405147

Syakila, A., Kroeze, C., & Slomp, C. P. (2010). Neglecting sinks for $N_2O$ at the earth's surface: Does it matter? *Journal of Integrative Environmental Sciences*, *7*(S1), 79–87. https://doi.org/10.1080/1943815x.2010.497492

Teh, Y. A., Silver, W. L., & Conrad, M. E. (2005). Oxygen effects on methane production and oxidation in humid tropical forest soils. *Global Change Biology*, *11*(8), 1283–1297. https://doi.org/10.1111/j.1365-2486.2005.00983.x

Tian, H., Yang, J., Xu, R., Lu, C., Canadell, J. G., Davidson, E. A., … Zhang, B. (2019). Global soil nitrous oxide emissions since the preindustrial era estimated by an ensemble of terrestrial biosphere models: Magnitude, attribution, and uncertainty. *Global Change Biology*, *25*(2), 640–659. https://doi.org/10.1111/gcb.14514

Urmann, K., Gonzalez-Gil, G., Schroth, M. H., Hofer, M., & Zeyer, J. (2005). New field method: Gas push−pull test for the in-situ quantification of microbial activities in the vadose zone. *Environmental Science & Technology*, *39*(1), 304–310. https://doi.org/10.1021/es0495720

Vant't Hoff, J. H., & Lehfeldt, R. A. (1899). *Lectures on theoretical and physical chemistry. Part 1. Chemical dynamics*. London: Edward Arnold.

Verchot, L. V., Davidson, E. A., Cattânio, J. H., & Ackerman, I. L. (2000). Land-use change and biogeochemical controls of methane fluxes in soils of eastern Amazonia. *Ecosystems*, *3*(1), 41–56. https://doi.org/10.1007/s100210000009

Verstraete, W., & Focht, D. (1977). Biochemical ecology of nitrification and denitrification. In M. Alexander (Ed.), *Advances in microbial ecology* (Vol. 1, pp. 135–214). Boston, MA: Springer.

Vieten, B. (2008). *$N_2O$ reduction in soils*. PhD thesis, University of Basel, Switzerland.

Wang, B., Brewer, P. E., Shugart, H. H., Lerdau, M. T., & Allison, S. D. (2019). Soil aggregates as biogeochemical reactors and implications for soil–atmosphere exchange of greenhouse gases—A concept. *Global Change Biology*, *25*(2), 373–385. https://doi.org/10.1111/gcb.14515

Wen, Y., Chen, Z., Dannenmann, M., Carminati, A., Willibald, G., Kiese, R., … Corre, M. D. (2016). Disentangling gross $N_2O$ production and consumption in soil. *Scientific Reports*, *6*, 36517. https://doi.org/10.1038/srep36517

Westermann, P. (1993). Temperature regulation of methanogenesis in wetlands. *Chemosphere*, *26*(1–4), 321–328. https://doi.org/10.1016/0045-6535(93)90428-8

Xu, X., Yuan, F., Hanson, P. J., Wullschleger, S. D., Thornton, P. E., Riley, W. J., … Tian, H. (2016). Reviews and syntheses: Four decades of modeling methane cycling in terrestrial ecosystems. *Biogeosciences*, *13*(12), 3735–3755. https://doi.org/10.5194/bg-13-3735-2016

Yamazaki, T., Yoshida, N., Wada, E., & Matsuo, S. (1987). $N_2O$ reduction by *Azotobacter vinelandii* with emphasis on kinetic nitrogen isotope effects. *Plant and Cell Physiology*, *28*(2), 263–271. https://doi.org/10.1093/oxfordjournals.pcp.a077292

Yamulki, S., Goulding, K. W. T., Webster, C. P., & Harrison, R. M. (1995). Studies on NO and $N_2O$ fluxes from a wheat field. *Atmospheric Environment*, *29*(14), 1627–1635. https://doi.org/10.1016/1352-2310(95)00059-8

Yan, Z., Liu, C., Todd-Brown, K. E., Liu, Y., Bond-Lamberty, B., & Bailey, V. L. (2016). Pore-scale investigation on the response of heterotrophic respiration to moisture conditions in heterogeneous soils. *Biogeochemistry*, *131*(1), 121–134. https://doi.org/10.1007/s10533-016-0270-0

Yang, W. H., McNicol, G., Teh, Y. A., Estera-Molina, K., Wood, T. E., & Silver, W. L. (2017). Evaluating the classical versus an emerging conceptual model of peatland methane dynamics. *Global Biogeochemical Cycles*, *31*(9), 1435–1453. https://doi.org/10.1002/2017GB005622

Yoshida, N., Matsuo, S., Yamazaki, T., & Wada, E. (1987). $N_2O$ Reduction by Azotobacter vinelandii with emphasis on kinetic nitrogen isotope effects. *Plant and Cell Physiology*, *28*(2), 263–271. https://doi.org/10.1093/oxfordjournals.pcp.a077292

Zarnetske, J. P., Haggerty, R., Wondzell, S. M., Bokil, V. A., & González-Pinzón, R. (2012). Coupled transport and reaction kinetics control the nitrate source-sink function of hyporheic zones. *Water Resources Research*, *48*(11), 1–15. https://doi.org/10.1029/2012WR011894

Zheng, J., & Doskey, P. V. (2015). Modeling Nitrous oxide production and reduction in soil through explicit representation of denitrification enzyme kinetics. *Environmental Science & Technology*, *49*(4), 2132–2139. https://doi.org/10.1021/es504513v

## SUPPORTING INFORMATION

Additional supporting information may be found online in the Supporting Information section.

**How to cite this article:** Sihi D, Davidson EA, Savage KE, Liang D. Simultaneous numerical representation of soil microsite production and consumption of carbon dioxide, methane, and nitrous oxide using probability distribution functions. *Glob Change Biol*. 2020;26:200–218. https://doi.org/10.1111/gcb.14855